What mechanisms explain the tropospheric drying associated with convective organization? Insights from cloud-resolving and last-saturation models

Camille Risi[1], Felix Langot[1], Esteban Nocet-Binois[1], and Caroline Muller[2]

[1]LMD, IPSL, CNRS, Paris, France
[2]ISTA

November 21, 2022

Abstract

In observations and cloud-resolving model (CRM) simulations, large-scale domains where convection is more aggregated (clustered into a smaller number of clouds) are associated with a drier troposphere. What mechanisms explain this drying? Hypotheses involve dynamical and microphysical processes. The goal of this study is to quantify the relative importance of these processes. We use a series of CRM simulations with different dynamical regimes and different kinds of convective organization forced by external forcings (isolated cumulonimbi, tropical cyclones, squall lines). We interpret the simulation results in the light of a hierarchy of simpler models (last-saturation model, analytical model). In CRM simulations, the troposphere is drier in the environment of more aggregated convection (tropical cyclones and squall lines). A last-saturation model is able to reproduce the drier troposphere even in absence of any microphysical processes or horizontal motions. Cloud intermittence is the key factor explaining this drying: when clouds are more intermittent, subsiding air parcels are more likely to encounter a cloud. An analytical model highlights the key role of the duration of convective systems. Remoistening by microphysical processes contributes to the moister troposphere when convection is less aggregated, though its importance is secondary smaller than that of intermittence. We suggest that the observed anti-correlation between convective aggregation and relative humidity may, at least partially, be mediated by the duration of convective systems.

What mechanisms explain the tropospheric drying associated with convective organization? Insights from cloud-resolving and last-saturation models

Camille Risi [1], Felix Langot [1], Esteban Nocet-Binois[1], Caroline Muller [1,2]

[1]Laboratoire de Meteorologie Dynamique, IPSL, CNRS, Ecole Normale Superieure, Sorbonne Universite, PSL Research University, Paris, France
[2]Institute of Science and Technology Austria, Klosterneuburg, Austria

Key Points:

- A simple last-saturation model captures the drier environment around the organized convection
- Cloud intermittence explains most of the humidity variations with the convective organization
- Remoistening by microphysical processes also contributes to the humidity variations.

Corresponding author: Camille RISI, `crisi@lmd.ipsl.fr`

Abstract

In observations and cloud-resolving model (CRM) simulations, large-scale domains where convection is more aggregated (clustered into a smaller number of clouds) are associated with a drier troposphere. What mechanisms explain this drying? Hypotheses involve dynamical and microphysical processes. The goal of this study is to quantify the relative importance of these processes. We use a series of CRM simulations with different dynamical regimes and different kinds of convective organization forced by external forcings (isolated cumulonimbi, tropical cyclones, squall lines). We interpret the simulation results in the light of a hierarchy of simpler models (last-saturation model, analytical model). In CRM simulations, the troposphere is drier in the environment of more aggregated convection (tropical cyclones and squall lines). A last-saturation model is able to reproduce the drier troposphere even in absence of any microphysical processes or horizontal motions. Cloud intermittence is the key factor explaining this drying: when clouds are more intermittent, subsiding air parcels are more likely to encounter a cloud. An analytical model highlights the key role of the duration of convective systems. Remoistening by microphysical processes contributes to the moister troposphere when convection is less aggregated, though its importance is secondary smaller than that of intermittence. We suggest that the observed anti-correlation between convective aggregation and relative humidity may, at least partially, be mediated by the duration of convective systems.

Plain Language Summary

Water vapor in the Earth's atmosphere is the main contributor to the greenhouse effect. As global climate warms, the atmospheric water vapor content increases, amplifying the warming. This so-called water vapor feedback is the largest feedback at play in the context of global warming. This feedback can be modulated by changes in atmospheric relative humidity. Previous studies have suggested that, as climate warms, tropical storms could become more aggregated into a smaller number of larger storms, and that more aggregated storms lead to a drier troposphere. This would yield a negative climate feedback partially opposing the water vapor feedback. The goal of this paper is to understand by which mechanisms more aggregated storms lead to a drier atmosphere. Using high-resolution simulations (between 750 and 4km in horizontal) of isolated showers, squall lines and cyclones, combined with theoretical models, we show that the main mechanism is cloud intermittence, which is related to the life duration of storms. When storms are more aggregated, they live longer, so clouds are less intermittent, and so subsiding air parcels around clouds are less likely to be remoistened by another cloud during their descent.

1 Introduction

1.1 Convective organization and importance for climate

Deep convection in the atmosphere, which manifests itself as storms, is responsible for most of the precipitation in the tropics. It can take the form of isolated, small-scale (about 10 km) and short-lived (about 1 hour) cumulonimbus clouds, or "organize" into bigger convective systems. "Organized" convective systems are characterized by their large size (e.g. >100 km) and by a meso-scale circulation and an internal structure (Houze Jr & Betts, 1981). For example, squall lines are arcs of convective cores, typically preceded by gust fronts and followed by an extended region of stratiform clouds (Gamache & Houze, 1981). Tropical cyclones are the most spectacular manifestations of convective organization, with scales up to 1000 km, and a circular structure comprising an eye, deep eyewall clouds and spiraling rainbands with extensive stratiform clouds (Houze, 2010). One measure of convective organization is the degree of spatial aggregation, which quantifies the extent to which convection in a large-scale domain (e.g. 100-1000 km) is clustered into a small number of convective system (Tobin et al., 2012).

Mesoscale convective organization matters for climate because different types of convective organization have different impacts on their large-scale environment, in particular tropospheric relative humidity (RH). For a given rain rate in average over a large-scale domain, states with more aggregated convection are associated with a drier environment both in observations (Tobin et al., 2012) and in cloud resolving model (CRM) simulations (Bretherton et al., 2004). This favors enhanced longwave emission to space. In turn, convective aggregation is favored over warmer sea surface temperatures in CRM simulation (Wing et al., 2017). Therefore, convective organization can act as a climate feedback in the context of global warming (Mauritsen & Stevens, 2015; Bony et al., 2016). Meso-scale convective organization may be a key missing component in global climate models used for projections (Mapes & Neale, 2011; Tobin et al., 2013; Moncrieff, 2019).

1.2 What mechanisms explain the drier troposphere when convection is more aggregated?

Before being able to assess the possible impact of convective organization on climate and account for it in climate models, it is necessary to better understand the mechanisms at play. In this study, we focus on this question: what mechanisms explain the observed drier troposphere when convection is more aggregated?

First of all, is the relationship between convective aggregation and RH a causal relationship? The observed anti-correlation between convective aggregation and tropospheric RH could be due to their simultaneous correlation with large-scale conditions. Indeed, large, long-lived convective systems are more frequent at the edges of the inter-tropical convergence zone (Roca et al., 2014). In these regions, the large-scale circulation advects drier air from higher latitudes. Dry air intrusions have been shown to favor the organization of convection into large systems such as squall lines (Diongue et al., 2002; Roca et al., 2005). Therefore, large-scale advection of dry air could favor both a dry troposphere and aggregated convection. However, even in CRM simulations without any large-scale circulation or horizontal advection, the troposphere is drier when convection is more aggregated (Bretherton et al., 2005). This suggests that convective aggregation impacts the tropospheric RH. In the following, we will review hypotheses that have been proposed to explain this impact (fig 1).

1. Hypothesis #1: microphysical moistening (fig 1 purple). Aggregated convection could be associated with a reduced moistening of the environment by microphysical processes (Tobin et al., 2012). When convection is more aggregated into a smaller number of clouds, the interface between clouds and their environment is smaller ((Beucler et al., 2020), fig 1b, purple rays). Microphysical processes that moisten the surrounding air along this interface (detrainment of cloud droplets and ice crystals, rain evaporation, snow sublimation) are thus less effective.
2. Hypotheses #2: dynamical processes. Purely dynamical processes could explain the drier troposphere. To first order, the RH of an air parcel is controlled by the altitude at which it has last saturated (Sherwood, 1996; Sherwood et al., 2010). This is called the last-saturation paradigm. In clouds, the air is saturated (RH=1, fig 1 purple squares). Around clouds, the air slowly subsides, adiabatically warms, and thus its RH decreases (fig 1 multicolored arrows going from purple towards blue, green, yellow, orange and red). Far from clouds, the air subsides from the upper troposphere and is thus very dry (fig 1 orange). This paradigm is very skillful to explain the large-scale distribution of free-tropospheric RH in response to the large-scale circulation ((Pierrhumbert & Roca, 1998; Dessler & Sherwood, 2000)). We hypothesize that this paradigm can also be skillful to explain the RH at the meso-scale around clouds.

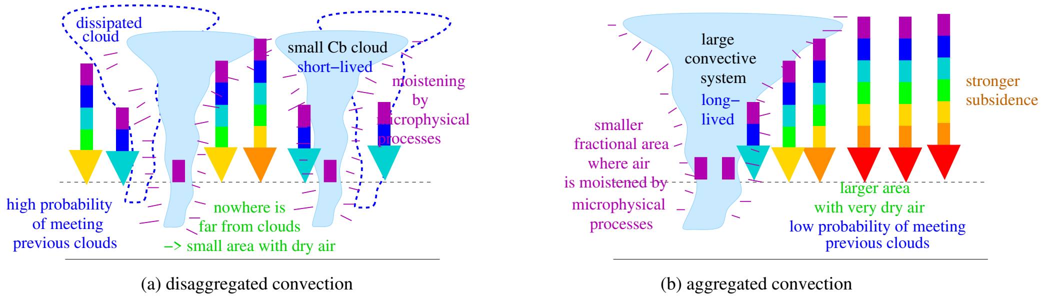

Figure 1. Schematic illustrating the 4 hypotheses proposed to explain the drier troposphere when convection is more aggregated. We show the processes controlling the RH at a given mid-tropospheric level (horizontal dashed line) in a disaggregated state (a) and aggregated state (b). The domain-mean rain rate and cloud fraction are the same in both cases. The multicolored arrows represent the subsiding air parcels, which are saturated as they leave clouds (purple) and dry as they descend (colors changing to blue, green, yellow and red). The purple rays around clouds show the moistening by microphysical processes. The dashed blue clouds show previous clouds that have dissipated. Hypothesis #1 (purple): moistening of the environment by microphysical processes is more effective when the number of clouds is larger, due to a larger interface area between clouds and the environment. Hypothesis #2a (green): when convection is more aggregated, areas around large convective systems that are far from any clouds are larger, so the areas with very dry air, falling from the upper troposphere without meeting any cloud, is larger. Hypothesis #2b (blue): when convection is more aggregated, convective systems are larger and longer lived. The air has a lower probability of having met previous clouds during its descent. Hypothesis 2c (brown): when convection is more aggregated, the subsidence around clouds is larger, reducing the probability of air parcels to meet clouds.

(a) Hypothesis #2a: spatial arrangement. When convection is more aggregated, a larger fraction of the domain is far from any clouds. The domain-mean is thus drier ((Romps, 2021), fig 1b green).

(b) Hypothesis #2b: cloud intermittence (fig 1 blue): while hypothesis #2a is framed in terms of spatial aggregation, it could also be extended to the temporal distribution of clouds. The RH distribution within a domain can be understood as a balance between the time scale of subsidence and the time scale at which air parcels encounter clouds (Sherwood et al., 2006). This time scale may depend on convective organization (Ryoo et al., 2009). When convection is disaggregated, isolated cumulonimbi grow and dissipate randomly across the domain (fig 1a). Clouds are more intermittent. If an air parcel falls outside a cloud, it is likely that newly-formed clouds will grow at its location during its descent. In contrast, when convection is more aggregated, convective systems are longer lived. If an air parcel falls outside a cloud, it is less likely to meet a newly-formed cloud during its descent (fig 1b).

(c) Hypothesis #2c: subsidence velocity. When convection is more aggregated, the subsidence velocity in the environment could be larger. CRM studies of self-aggregation show a larger subsidence velocity in the environment due to the effect of water vapor and cloudiness on longwave radiation (Bretherton et al., 2005; Muller & Held, 2012). This enhanced subsidence is part of a feedback loop that favors self-aggregation of convection. A larger subsidence reduces the probability of descending air parcels to meet clouds (Sherwood et al., 2006).

Table 1. Overview of the 6 simulations: type of convective organization, horizontal domain and resolution, vertical grid, forcing, domain-mean rain rate, domain-mean and standard deviation of precipitable water (PW).

Simulation name	Convective organization	Horizontal domain (km)	Horizontal resolution (km)	Vertical grid (number of levels)	Large-scale ascent	Additional forcing	Domain-mean rain rate (mm/d)	PW mean ± standard deviation (kg/m2)
Cb	pop-corn	96×96	0.750	96	no	none	2.5	56±2
Cb+	pop-corn	96×96	0.750	96	yes	none	8.5	69±4
TC	tropical storm	512×512	4	96	no	rotation	3.0	47±16
TC+	tropical cyclone	512×512	4	96	yes	rotation	9.4	49±20
SL	squall line	256×256	2	64	no	wind shear	3.2	44±7
SL+	squall line	256×256	2	64	yes	wind shear	8.3	51±6

1.3 Goal and approach

The goal of this study is to test these different hypotheses, and quantify their relative importance. To do so, we run CRM simulations with different kinds of convective organization: isolated cumulonimbi, cyclones, or squall lines (section 2). In reality, convective organization typically occurs as a response to external forcing (Houze, 2004). Therefore, the realism of aggregated states obtained through from self-aggregation have been questioned (Stein et al., 2017; Muller et al., 2022). This is why here we consider aggregated states driven by external forcings. In addition, organized convection is typically observed in regions of large-scale ascent (Tan et al., 2013; Jakob et al., 2019). Therefore, we run CRM simulations both in radiative-convective equilibrium (RCE) and with prescribed large-scale ascent (Warren et al., 2020; Risi et al., 2021).

To understand the mechanisms controlling RH in the CRM simulations, we design a hierarchy of simpler models (Held, 2005).

- First, we develop a simple last-saturation model that accounts for remoistening processes to quantify the relative importance of the microphysical (hypothesis #1) and dynamical (hypotheses #2) processes (section 3).
- Second, we propose an even simpler, analytical models, to estimate the microphysical and dynamical contributions to the changes in relative humidity and to provide a more detailed physical interpretation of these contributions (section 4).

2 Cloud Resolving Model simulations and their simulated humidity

2.1 Description of the simulations

We run 6 simulations (table 1) with two regimes of large-scale circulation (section 2.1.3) and three kinds of convective organization: isolated cumulonimbi, tropical cyclones (section 2.1.4) and squall lines (2.1.5).

2.1.1 Cloud Resolving model

We use the non-hydrostatic Cloud Resolving Model (CRM) System for Atmospheric Modeling (SAM) ((Khairoutdinov & Randall, 2003)), version 6.10.9. This model solves anelastic conservation equations for momentum, mass, energy and water, which is present in the model under six phases: water vapor, cloud liquid, cloud ice, precipitating liquid, precipitating snow, and precipitating graupel. We use the bulk, mixed-phase microphysical parameterization from (Thompson et al., 2008). The model version is the same as in (Risi et al., 2020, 2021).

2.1.2 Radiative-convective equilibrium simulations.

Simulations are three-dimensional, with a doubly-periodic domain. They are run in radiative-convective equilibrium over an ocean surface. The sea surface temperature (SST) is 30°C. Diurnal cycles are ignored, diurnal-mean solar influx is applied. The simulations are run during 50 days. The last 10 days of simulation are analyzed with three-dimensional instantaneous output files every 30 minutes.

2.1.3 Large-scale circulation

Organized convection is typically observed in regions of large-scale ascent (Tan et al., 2013; Jakob et al., 2019). Therefore, in half of our simulations we impose a large-scale vertical ascent with a cubic shape, reaching -40 hPa/d at 400 hPa and 0 hPa/d at the surface and above 100 hPa (Risi et al., 2020, 2021). From this large-scale ascent, large-scale tendencies in temperature and specific humidity are calculated and added in a horizontally uniform way to all grid points of the domain. The resulting cooling destabilizes the troposphere and the resulting moistening reduces the drying effect of entrainment, both resulting in enhanced domain-mean rain rate (Risi et al., 2020, 2021; Warren et al., 2020).

Without large-scale ascent, the domain-mean rain rate ranges from 2.5 mm/d to 3.2 mm/d depending on convective organization (table 1). With large-scale ascent, it ranges from 8.3 to 9.4 mm/d.

2.1.4 Set-up for the cyclone simulations

We use a doubly-periodic domain of 512 km×512 km with a horizontal resolution is 4 km and 96 vertical levels. This horizontal resolution is sufficient to properly simulate the internal structure of a cyclone (Gentry & Lackmann, 2010). Cyclones spontaneously develop in radiative-convective equilibrium simulations when some rotation is added (Khairoutdinov & Emanuel, 2013; Muller & Romps, 2018). Here the effect of rotation is added through a Coriolis parameter that corresponds to a latitude of 40°. Although no tropical cyclones are expected to form at such latitudes, a strong rotation allows us to simulate a small cyclone (Chavas & Emanuel, 2014) that can fit our small domain. This allows the simulation to remain computationally reasonable. The initial conditions are spatially homogeneous and one unique cyclone develops spontaneously through self-aggregation mechanisms after a few days. This is consistent with the time scale for cyclogenesis in other self-aggregation studies (Muller & Romps, 2018).

2.1.5 Set-up for the squall line simulations

We use a doubly-periodic domain of 256 km×256 km with a horizontal resolution is 2 km and 96 vertical levels. Squall lines spontaneously develop in radiative-convective equilibrium simulations when horizontal wind shear is added (Robe & Emanuel, 2001; Muller, 2013; Abramian et al., 2022). We add a horizontally uniform wind in the x direction that reaches 10 m/s at the surface and linearly decrease to 0 m/s up to 1 km. This uniform surface wind is subtracted when calculating surface fluxes, to avoid this simulation to have significantly higher surface fluxes. The radiative fluxes are imposed, because interactive radiation leads to some radiative feedbacks that disfavor the organization into squall lines. The convection quickly organizes into a line, after about one day of simulation.

2.2 Overview of the simulations

Simulations of isolated cumulonimbi, cyclones and squall lines are called "Cb", "TC" and "SL" respectively. Simulations with large-scale ascent are denoted with a "+" (table 1). Fig 2 shows snapshots of precipitable water at arbitrary time steps for the 6 simulations. Videos of these simulations are available in SI (SI videos V1). In absence of additional forcing, radiative-convective equilibrium simulations with or without large-scale ascent exhibit typical disaggregated, "pop-corn" convection, with at least 10 simultaneous isolated cumulonimbi in the domain (fig2 a-b).

When rotation is added, convection aggregates into a tropical storm in the case without large-scale ascent (fig2c), and into a category 4 tropical cyclone in the case with large-scale ascent (fig2c). The standard deviation of precipitable water can be considered a proxy for the degree of convective aggregation (Wing et al., 2016). When rotation is added, the standard deviation rises from 2 to 16 kg/m^2 and from 4 to 20 kg/m^2 without and with large-scale ascent respectively (table 1), confirming the much higher degree of aggregation in cyclone simulations relative to disaggregated simulations.

When wind shear is added, convection aggregates into squall lines (fig 2e-f). The standard deviation of precipitable water rises from 2 to 7 kg/m^2 and from 4 to 6 kg/m^2 without and with large-scale ascent respectively (table 1), confirming the higher degree of aggregation in squall line simulations relative to disaggregated simulations, although the increase is less dramatic than for tropical cyclone simulations.

2.3 Simulated domain-mean humidity

Most simulated relative humidity profiles show a trimodal structure with maxima corresponding to the 3 main levels of convective outflows: in the boundary layer, near the freezing level, and in the upper troposphere (fig 3a). This is consistent with observations (Johnson et al., 1999). Whatever the convective organization, simulations with large-scale ascent are typically moister than simulations without large-scale ascent throughout the whole troposphere, except for TC simulations below 3 km (fig 3c). The moister troposphere associated with more large-scale ascent and heavier rain rates is also consistent with observations (Bretherton et al., 2004).

Whatever the regime of large-scale ascent and the convective organization type (cyclone or squall line), organized convection is associated with a drier troposphere at all levels (fig 3d). This is consistent with observations (Tobin et al., 2012) and previous simulations (Bretherton et al., 2005). Aggregated simulations are drier even though they have slightly higher rain rates than their disaggregated counterparts (table 1). This confirms that even with realistic, forced types of convective organization, the relationship between aggregation and tropospheric humidity holds.

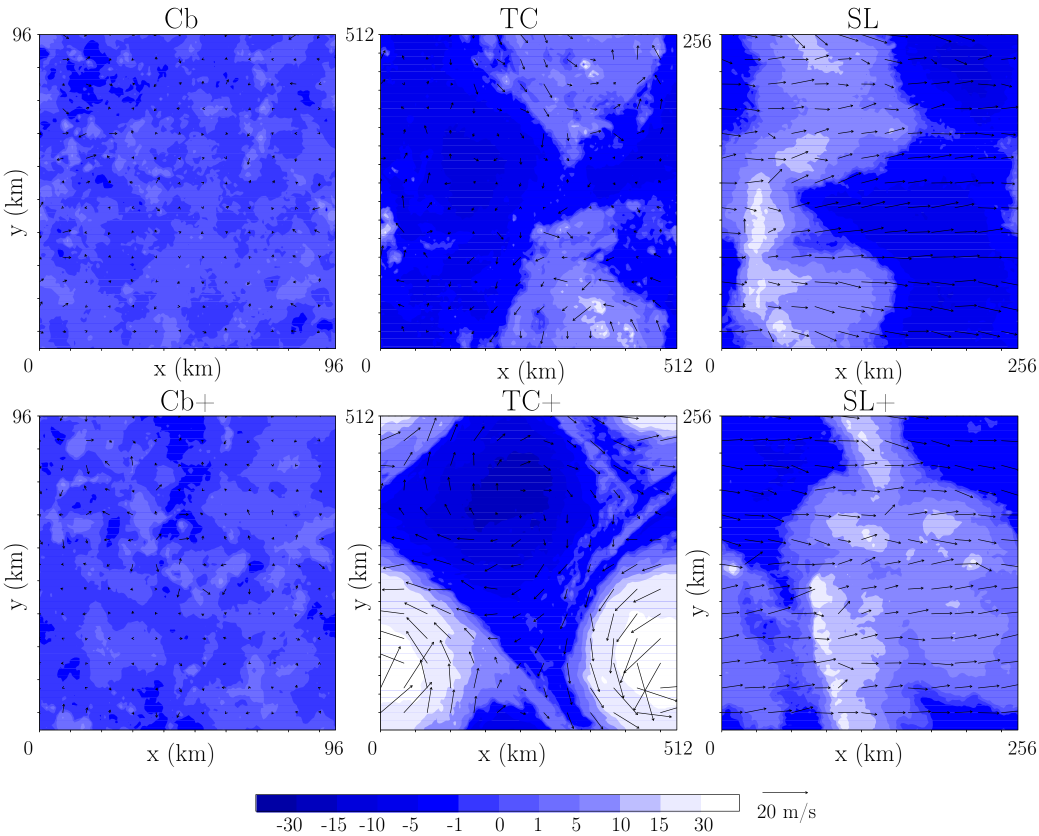

Figure 2. Maps of the precipitable water anomaly for arbitrary snapshots for the 6 different simulations. Vectors indicate the near-surface wind field. The domain is doubly periodic: clouds at the right-hand side of the domains connect with those at the left-hand side, and clouds at the upper side of the domains connect with those at the lower side.

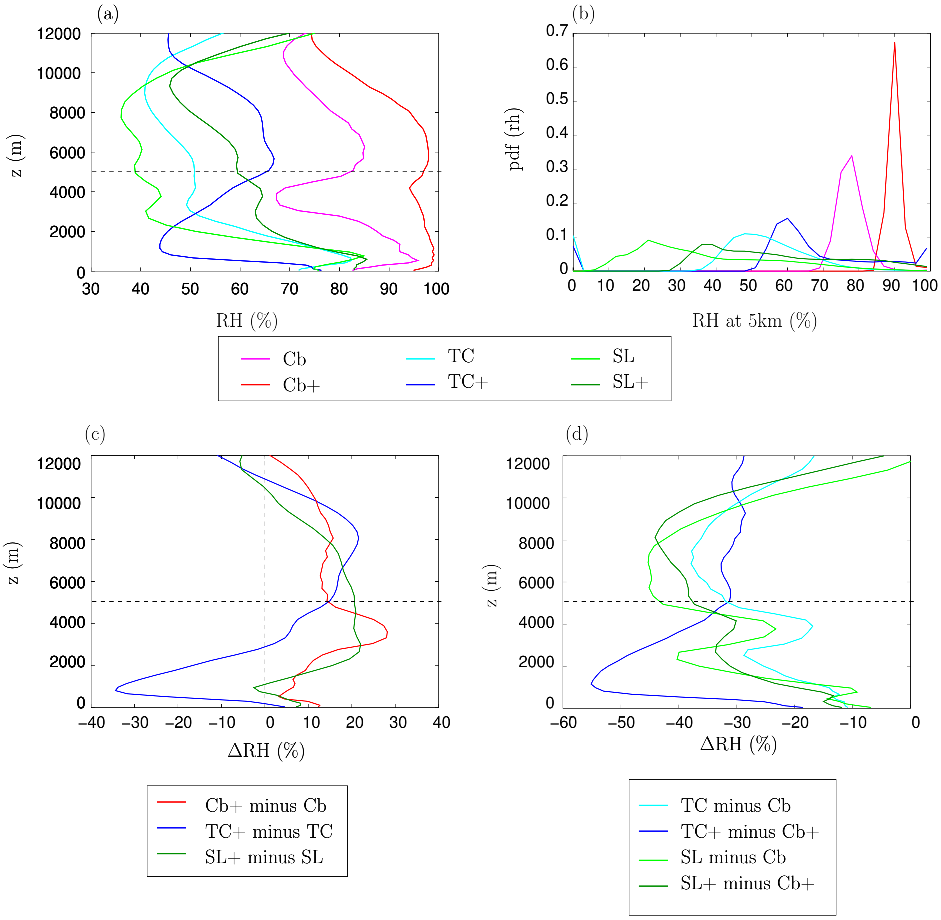

Figure 3. (a) Domain-mean relative humidity profiles for the 6 simulations. (b) Probability distribution of RH at 5 km. Differences in domain-mean RH profiles between simulations with and without large-scale ascent. (c) Differences in domain-mean RH profiles between simulations of organized convection and pop-corn convection. The horizontal lines highlights the 5 km horizontal level.

The probability distribution of RH in the mid-troposphere shows a unimodal distribution (fig 3b), consistent with (Ryoo et al., 2009). The distribution is broader for more aggregated simulations, consistent with the larger standard deviation of precipitable water (table 1). For aggregated simulations, the most frequent RH is dry, consistent with a large fraction of the domain that experiences little convection. The tail for larger RH corresponds to the fraction of the domain that experiences more convection. When RH is drier, it is the dry peak that is drier. This is consistent with the observation that in more aggregated states, it is the environment outside convection that is drier (Tobin et al., 2012).

Now we aim at explaining the physical mechanisms responsible for the drier troposphere when convection is more aggregated. With this aim, we develop a last-saturation model.

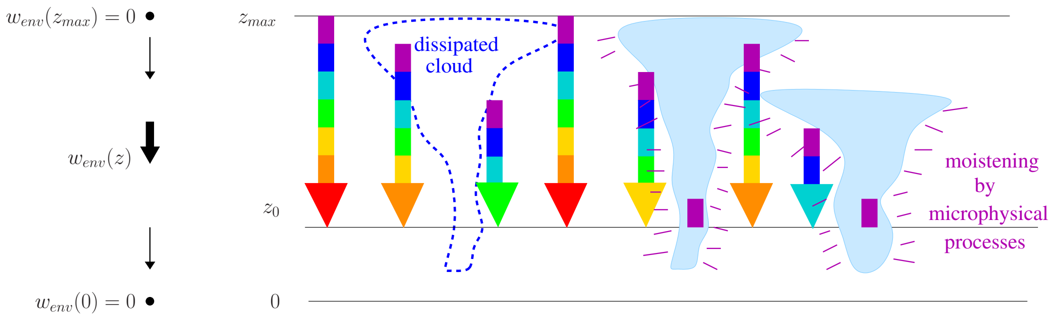

Figure 4. Schematic illustrating the last-saturation model.

3 Last-saturation model

We hypothesize that the main reason for the drier troposphere in aggregated convection is because air parcels descend from higher up without encountering any cloud. This is why we build our model based on the last-saturation paradigm (Sherwood, 1996). Our approach is inspired by the probabilistic model of (Sherwood et al., 2006).

3.1 Description of the model

3.1.1 Last-saturation model with vertical back-trajectories

According to the last-saturation paradigm, the specific humidity of a parcel is at saturation in clouds and is conserved as it subsides outside clouds (fig 4). Therefore, the RH of an air parcel at instant t and in the grid box x, y, z_0 depends on the altitude where it was last saturated, z_{last}:

$$h_{last}(t, x, y, z_0) = \frac{q_{sat}(z_{last}(t, x, y, z_0))}{q_{sat}(z_0)} \tag{1}$$

where q_{sat} is the specific humidity at saturation, which is a function of temperature and pressure, which are both functions of altitude. Here we assume that the temperature is temporally and horizontally uniform. This approximation is justified since in the tropics temperature homogenizes very quickly (Bretherton & Smolarkiewicz, 1989). q_{sat} is thus a function of altitude only.

We assume that in the environment, air parcels slowly subside with a vertical velocity $w_{env}(z)$ that is temporally and horizontally uniform (fig 4). In reality, w may vary in space and time. This hypothesis is a strong simplification which will be discussed in section 3.4. The $w_{env}(z)$ profile is calculated as:

$$w_{env}(z) = \frac{\sum_{t,x,y} w(t, x, y, z) \cdot U(t, x, y, z)}{\sum_{t,x,y} U(t, x, y, z)} + w_{LS}(z)$$

where $w(t, x, y, z)$ is the vertical velocity anomaly simulated by the CRM, $U(t, x, y, z)$ is 0 if the grid box is cloudy and 1 otherwise; $w_{LS}(z)$ is the large-scale vertical velocity profile. A grid box is considered cloudy if its total condensate content (liquid + ice) is greater than 10^{-5}g/kg. Results are not very sensitive to this threshold.

At each instant and grid point t, x, y, z_0, we build a back-trajectory that describes how altitude z_{traj} evolves as time t_{traj} goes back, with time step dt (typically 30 minutes):

$$z_{traj}(t,x,y,z_0,t_{traj}-dt) = z_{traj}(t,x,y,z_0,t_{traj}) - w_{env}(z)\cdot dt$$

The back-trajectory is continued until it reaches the level z_{max} where $w_{env}(z)$ first exceeds -10^{-4} m/s, to avoid calculating infinite back-trajectories. If the trajectory encounters a cloud in a given grid box and at some trajectory time-step t_{last}, the back-trajectory is stopped and the altitude is recorded as the last-saturation altitude:

$$z_{last}(t,x,y,z_0) = z_{traj}(t,x,y,z_0,t_{last})$$

If no cloud is encountered, then z_{last} is set to z_{max}.

Therefore, the RH can be calculated at all instants and all grid points, as long as enough time steps are available to calculate a back-trajectory up to z_{max}. The calculation is valid only in the free troposphere: in the boundary layer, surface evaporation becomes a key control of RH (Stevens, 2006).

3.1.2 Static version of the last-saturation model

According to the last saturation model, since back-trajectories go back both in altitude and time, the RH is expected to depend both on the vertical and temporal variability of clouds. To check the relative importance of the vertical and temporal variability, we also design a "static" version of the last saturation model, in which back-trajectories are assumed to reach the upper troposphere instantaneously. At each instant and grid point, $z_{last}(t,x,y,z_0)$ is simply the lowest cloud above z_0. This is equivalent to neglecting the temporal variability of clouds, or assuming that the time scale of subsidence is much shorter than that between two clouds.

3.1.3 Accounting for remoistening by microphysical processes

To quantify the possible role of microphysical processes, a moistening tendency is added when the subsiding air parcels are outside clouds. The final relative humidity of the air parcel arriving at z_0 is:

$$h(t,x,y,z_0) = \frac{q_f(t,x,y,z_0)}{q_{sat}(z_0)}$$

where $q_f(t,x,y,z_0)$ is the specific humidity of the subsiding air parcel when it arrives at z_0:

$$q_f(t,x,y,z_0) = q_{sat}(z_{last}(t,x,y,z_0)) + \sum_{t_{traj}=t}^{t_{last}+dt} \left(\frac{dq}{dt}\right)_{remoist}(z_{traj})\cdot dt$$

where $\left(\frac{dq}{dt}\right)_{remoist}$ is the remoistening term affecting the descending air parcel. In reality, microphysical remoistening is likely a function of distance to cloud. But for the sake of simplicity, and for consistency with w_{env}, we assume that this remoistening term is horizontally and temporally uniform, depending on altitude only. This strong assumption will be discussed in section 3.4. We diagnose the remoistening term as a residual from the moisture budget in average over all non-cloudy air parcels:

$$\left(\frac{\partial q}{\partial t}\right)_{remoist,env} = max\left(0, \left[\frac{\partial q}{\partial t}\right]_{env} + w_{env}\cdot\left[\frac{\partial q}{\partial z}\right]_{env}\right) \quad (2)$$

where $[.]_{env}$ stands for the average over all non-cloudy air parcels. This remoistening term includes the moistening tendency by microphysical processes (evaporation of rain and cloud droplets, sublimation of ice crystals, snow and graupel), but also the remoistening by horizontal advection or by sub-grid scale mixing. It may also include the impact of co-variations between w and $\frac{\partial q}{\partial z}$. While the microphysical term is directly available from the outputs, the other terms would be more complicated to diagnose. This is why we calculate $\left(\frac{\partial q}{\partial t}\right)_{remoist,env}$ as a residual.

3.1.4 Method to decompose humidity differences

The goal of this last-saturation model is to quantify the contributions of different processes to the RH differences between pairs of simulations: $\Delta h = h_2 - h_1$, where subscripts 1 and 2 denote simulations.

We have 3 predictions of the RH for each simulations:

1. prediction with the last-saturation model with the remoistening term (section 3.1.3): $h_{dyn,remoist}$
2. prediction with the last-saturation model without the remoistening term (section 3.1.1): h_{dyn}
3. prediction with the static version of the last-saturation model (section 3.1.2): h_{stat}.

The RH of each simulation can thus be decomposed as:

$$h \simeq h_{dyn,remoist} = (h_{dyn,remoist} - h_{dyn}) + (h_{dyn} - h_{stat}) + h_{stat}$$

The first term represents the effect of remoistening and the second term represents the effects of the temporal variations in cloudiness. Further, we note h_{dyn2,w_1} the prediction with the last-saturation model without the remoistening term for simulation 2 but with $w_{env}(z)$ from simulation 1, and $h_{stat2,q_{s1}}$ the prediction with the static version of the last-saturation model for simulation 2 but with $q_{sat}(z)$ from simulation 1. We can thus decompose the RH difference between the 2 simulations into 5 contributions:

$$\Delta h = \Delta\left(h_{dyn,remoist} - h_{dyn}\right) + (h_{dyn2} - h_{dyn2,w_1}) + (h_{stat2} - h_{stat2,q_{s1}}) + (h_{stat2,q_{s1}} - h_{stat1})$$

$$+ \left(h_{dyn2,w_1} - h_{dyn1} - \Delta h_{stat}\right)$$

The 5 contributions are:

1. difference in the remoistening outside clouds: $\Delta\left(h_{dyn,remoist} - h_{dyn}\right)$,
2. difference in the subsidence velocity outside clouds $w_{env}(z)$: $h_{dyn2} - h_{dyn2,w_1}$,
3. difference in the thermal structure of the troposphere $q_{sat}(z)$: $h_{stat2} - h_{stat2,q_{s1}}$,
4. difference in the cloud fraction profile: $h_{stat2,q_{s1}} - h_{stat1}$,
5. difference in the cloud intermittence: $h_{dyn2,w_1} - h_{dyn1} - \Delta h_{stat}$. This represents the difference in the last-saturation prediction from which the effects of the differences in subsidence velocity, cloud fraction profile and thermal structure are subtracted.

3.2 Validation of the last-saturation model

The last-saturation model with the remoistening term captures to first order the RH profiles (fig 5a). It captures the moister RH with large-scale ascent in most of the troposphere (fig 5c) and the drier RH for aggregated simulations (fig 5d).

The predicted probability distributions of RH are not as smooth as those simulated by the CRM (fig 5b). Consistent with the CRM (fig 3b), the distributions for the aggregated simulations show a peak for dry RH, and the variations in domain-mean RH are associated with variations in the position of the dry peaks. However, the predicted distributions for Cb and Cb+ are too broad relative to those simulated by the CRM, while it is the opposite for SL and SL+. Hereafter, we will focus on the domain-mean RH.

The correlation across the different simulations between predicted and CRM RH is above 0.95 throughout the troposphere below 8 km (fig 6a, red). The slope of the corresponding linear relationship around 0.9 shows that the predicted RH is very similar to the CRM RH, though slightly underestimated by about 10% (fig 6b, red). Given the simplicity of this model, we consider that this agreement is sufficient to use this model to investigate the mechanisms controlling tropospheric RH.

Without the remoistening term, the skill of the prediction to capture the CRM RH is slightly lower than with the remoistening term. The correlation between predicted and CRM RH ranges from 0.7 to 0.95, and the predicted RH is underestimated relative to the CRM RH by about 10 to 20% (fig 6a-b green). Yet, given the simplicity of this model, the skill is surprisingly good (fig 6c, empty squares). This shows that the moistening by microphysical processes around clouds (hypothesis #1) is not the first order process controlling the RH.

Predictions with the static version of the last-saturation model are much less skillful to capture the CRM RH, with much weaker correlation coefficients (fig 6a blue). The predicted RH values are unrealistically low, below 10% (fig 6c, empty circles). The differences between simulations are underestimated, with a slope between predicted and CRM RH below 0.2 (fig 6b, blue). This shows that the cloud intermittence, not just the spatial arrangement of clouds, is key to determine the RH.

We now use the predictions by the three versions of the model to decompose the RH difference between simulation pairs.

3.3 Decomposing the humidity differences

3.3.1 Humidity differences associated with large-scale circulation

We first test our decomposition approach to understand why the troposphere is moister in case of large-scale ascent. Since the latter is better understood, this serves as a sanity check for our decomposition approach.

In the Cb and TC simulations, the main driver for the moister free troposphere in case of large-scale ascent is the larger cloud intermittence. In case of large-scale ascent, clouds are more intermittent, which increases the probability of air parcels to meet a cloud during their descent. This is consistent with the framework of (Sherwood et al., 2006), where the RH depends on the relative time scales of the subsidence and of the remoistening by clouds. In the SL simulations, in contrast, the main driver for the moister free troposphere in case of large-scale ascent is the more efficient moistening in the environment. The environment-mean moistening tendency is larger for SL+ than for SL (fig 8a), maybe due to stronger detrainment from a more intense squall line. In the cyclone and squall line simulations, the cloud fraction also contributes to the moistening (fig 7, green).This is because the cloud fraction is larger in case of large-scale ascent (fig 8b), enhancing the probability to meet clouds.

We notice that for all organization types, the environment subsides faster in case of large-scale ascent (fig 8c). This may sound counter-intuitive. This is because in case of large-scale ascent, the overturning circulation between the cloudy regions and their environment is more intense. This contradicts the idea that the subsidence velocity in the environment is constrained by the radiative cooling that varies little (Craig, 1996;

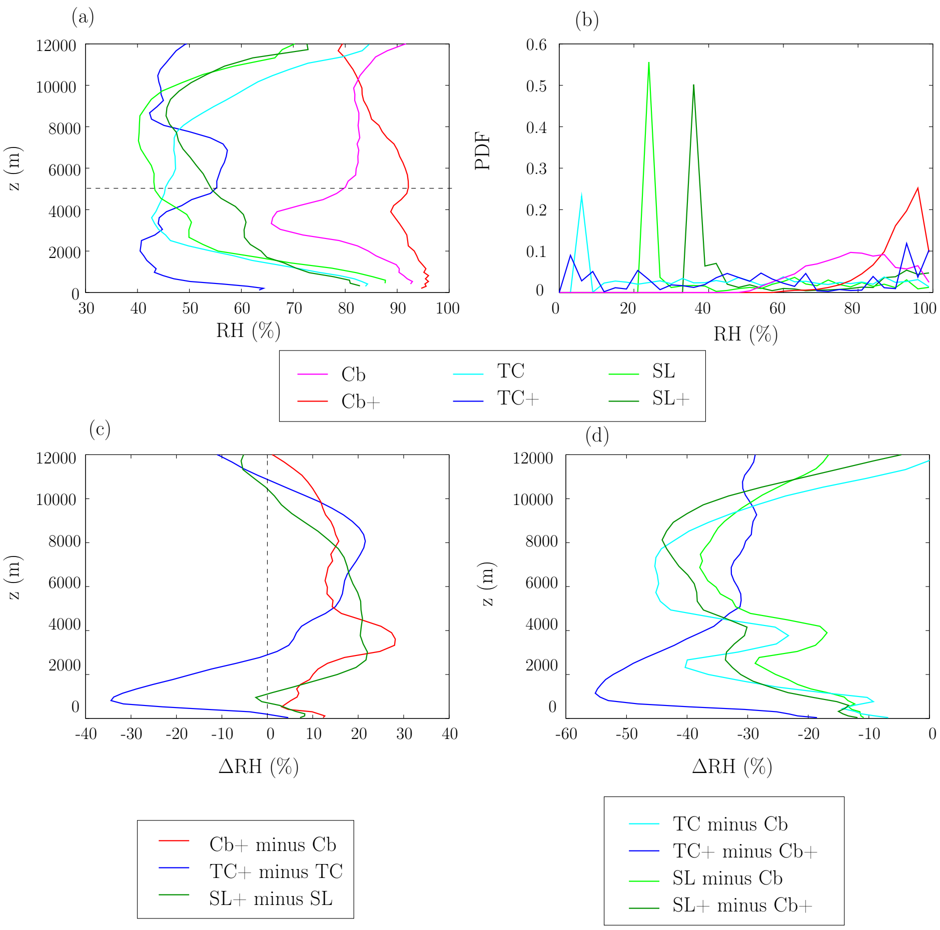

Figure 5. Same as 3 but for the last-saturation model with the remoistening term.

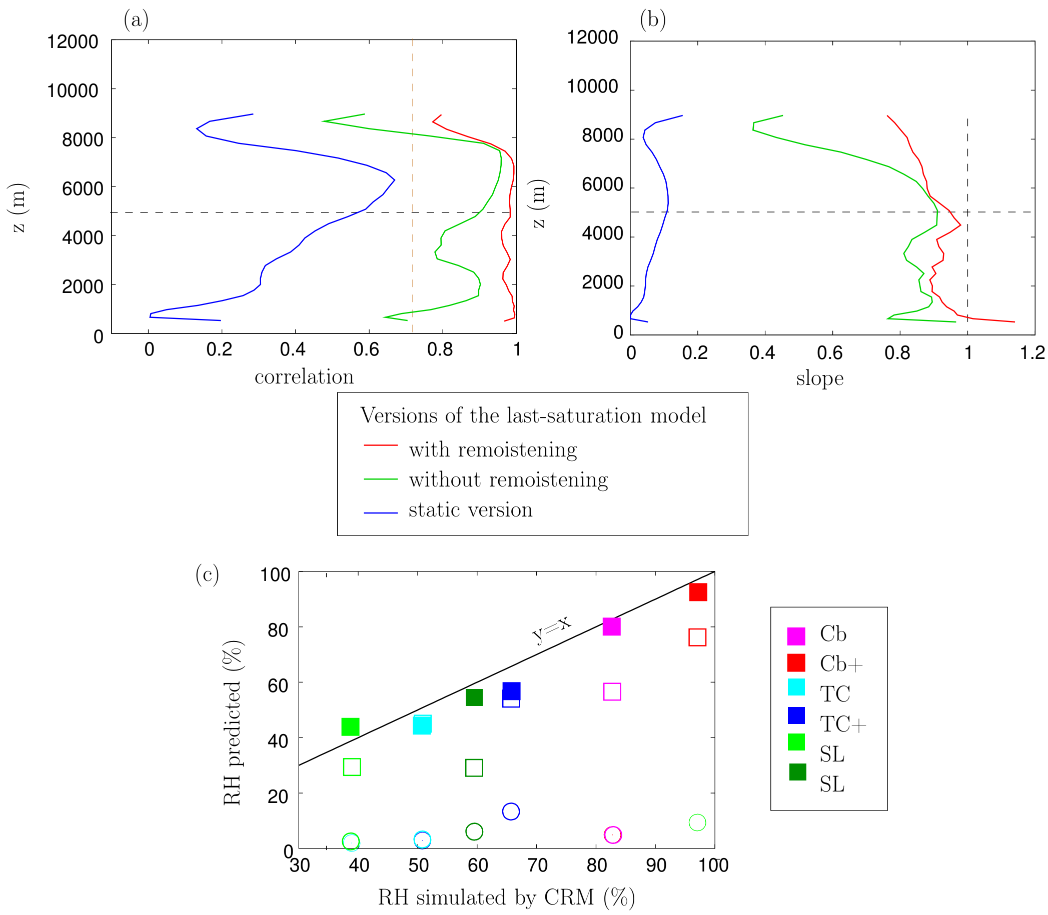

Figure 6. (a) Correlation coefficient as a function of altitude between the domain-mean RH predicted by the last-saturation model with remoistening (red), without remoistening (green) and in its static version (blue), and that simulated by the CRM, across the 6 simulations. The vertical dashed brown line indicates the correlation threshold for statistical significance at 90%. (b) Same as (a) but for the slope of the linear relationships. (c) Scatter plot of the domain-mean RH at 5km predicted by the last-saturation model with remoistening (full squares), without remoistening (empty squares) and in its static version (empty circles), as a function of that simulated by the CRM.

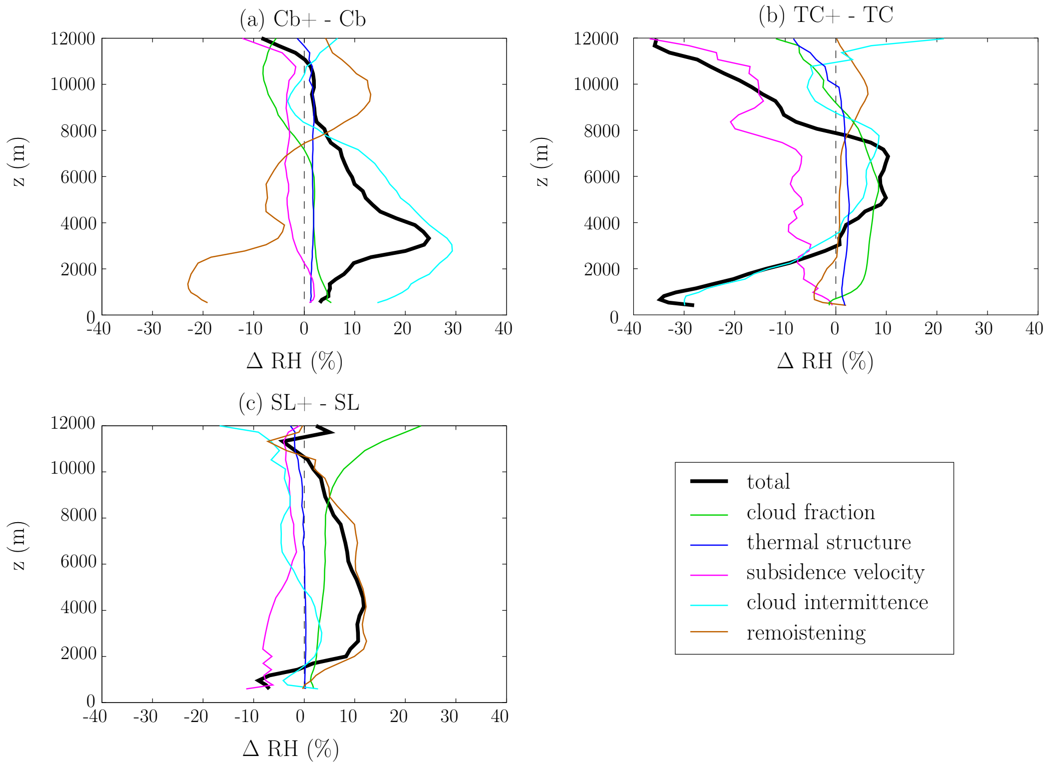

Figure 7. Decomposition of the total RH difference into its 5 contributions, for Cb+ minus Cb (a), TC+ minus TC (b) and SL+ minus SL (c): total difference (black), cloud fraction contribution (green), thermal structure (blue), subsidence velocity (magenta), cloud intermittence (cyan), remoistening by microphysical processes (brown).

Emanuel, 2019). In the environment, the more intense overturning circulation dominates over the large-scale ascent, leading to faster subsidence. As a consequence, air parcels have less time to meet clouds during their descent. The contribution of the subsident velocity in the environment thus opposes the changes of the free tropospheric humidity (fig 7b-c magenta). Note however that the realism of the simulated environment velocity in CRM simulations on limited, doubly-periodic domain can be questioned (Risi et al., 2021). It is sensitive to whether the prescribed effect of large-scale ascent is assumed horizontally uniform, as is the case here, or assumed concentrated in cloudy regions (Singh et al., 2019).

To summarize, the moister troposphere in case of large-scale ascent is due to different reasons for the different organization type: greater cloud intermittence or large remoistening around clouds.

3.3.2 Humidity differences associated with convective organization

For both organization type or dynamical regimes (except in the lower troposphere of the TC), the main driver of the tropospheric drying compared to Cb is the cloud intermittence (fig 9 cyan). When convection is disaggregated, clouds appear and die randomly across the domain. Air parcels that subside have a high probability of encountering these short-lived clouds. In contrast, when convection is more aggregated, air parcels that are away from the large, nearly stationary convective system have a very low probability to meet a cloud. Therefore, a larger portion of the domain is drier and the domain-

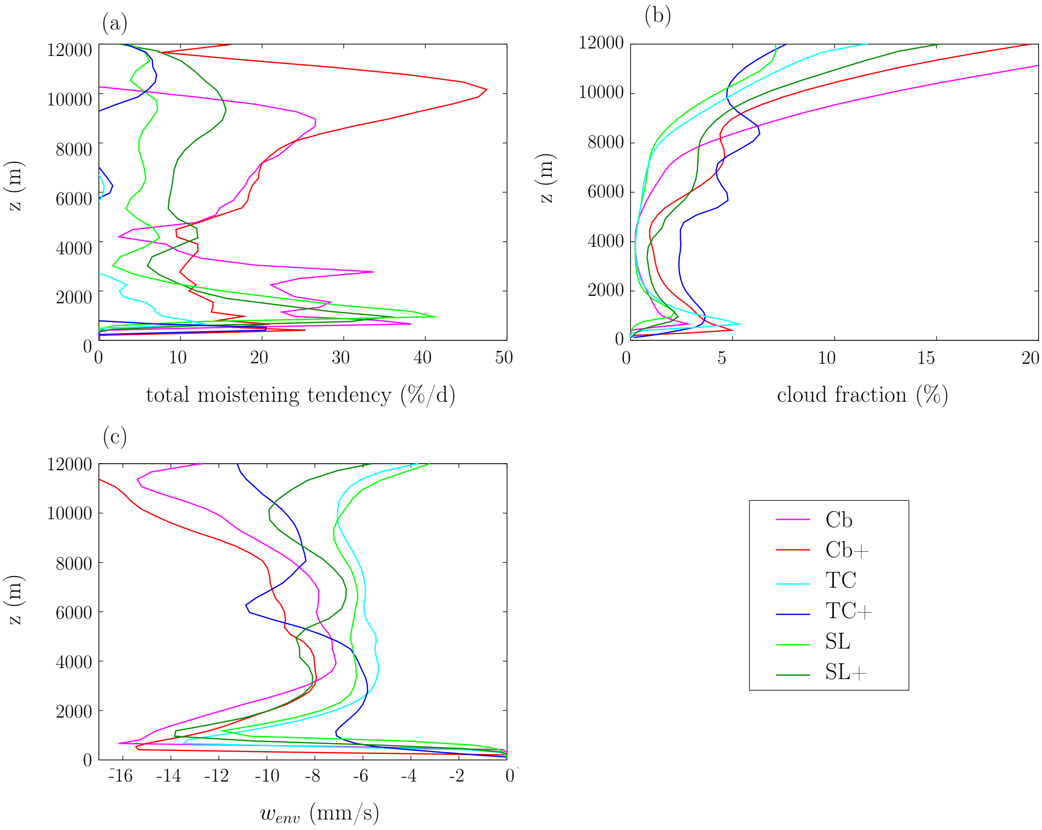

Figure 8. Vertical profiles of the moistening tendency (a), cloud fraction (b) and w_{env} (c) for the 6 simulations.

mean RH is lower (SI video V2 illustrating the importance of cloud intermittence). This validates our hypothesis #2b.

Remoistening around clouds has a smaller, but significantly positive contribution to the drying, for all cases except for SL+ minus Cb+ (fig 9 brown). This supports hypothesis #1, though it is not the main contribution. This result is consistent with the much larger moistening tendency simulated for Cb and Cb+ than for the other simulations (fig 8a). The larger contribution of remoistening around clouds when convection is more disaggregated can directly be tied to the number of convective systems, as will be shown in section 4.2.

The cloud fraction often has a small positive influence (fig 9 green). The subsidence velocity generally has a negative contribution to the drying (fig 9 magenta). When convection is more aggregated, the subsidence in the environment is slower (fig 8a). We can thus discard hypothesis #2c. This may sound counter-intuitive, given that subsidence in the environment has been suggested to be a driver of convective self-aggregation (Bretherton et al., 2005; Muller & Held, 2012). Rather, we find that the overturning circulation between cloudy regions and their environment is more intense in disaggregated cases. It is possible that the larger subsidence velocity for more aggregated cases is a specific result for self-aggregation cases that does not hold for aggregation driven by external forcing.

To summarize, the drier troposphere in case of more aggregated convection is robustly due to the reduced cloud intermittence, and to a lesser extent, to remoistening of the environment around clouds.

3.4 Discussion of a few approximations of the last saturation model

The simple model is based on many approximations, and we discuss here three of them.

First, we assume that the time step dt of 30 minutes is sufficient to correctly describe the temporal variability of the cloud field. To assess this assumption, we re-calculated the domain-mean RH using time steps dt of 24 hours, 6 hours, or 1 hour instead of 30 minutes (fig 10). We can see that as dt increases, RH tends towards that predicted in the static state. The temporal variability of the cloud field is less well captured at low temporal resolution. As dt decreases, the RH converges toward an asymptotic value (fig 10, dashed blue line). We can see that the RH predicted for $dt = 30$ minutes corresponds almost exactly to the asymptotic value. We thus conclude that the time step dt of 30 minutes is sufficient to correctly describe the temporal variability of the cloud field.

Second, we assumed that $w_{env}(z)$ and $\left(\frac{\partial q}{\partial t}\right)_{remoist,env}$ are horizontally and temporally uniform in the environment. In reality, both variables systematically vary as a function of the distance to the nearest cloud. To assess this effect, we calculated the vertical velocity and the moistening tendency not only as a function of altitude in average over all non-cloudy points (e.g. equation 2), but as a function of both altitude and of the distance to the nearest cloud (Figs 11 for w and 12 for $\left(\frac{\partial q}{\partial t}\right)_{remoist}$). We can see that air parcels subside the most strongly just around clouds, consistent with subsiding shells (Glenn & Krueger, 2014). This is where the moistening term is strongest. Therefore we expect that the larger subsidence velocity and the larger moistening tendency around clouds compensate each other, at least partially.

Third, we assumed that air parcels vertically subside and we neglect all horizontal motions. We expect that in reality, horizontal motions would favor the encounters of air parcels with clouds. In addition, air parcels are expected to diverge from cloud tops as they detrain. Therefore, parcels in the environment far from clouds will be interpreted as very dry by our last-saturation model, whereas in reality some of them may have lat-

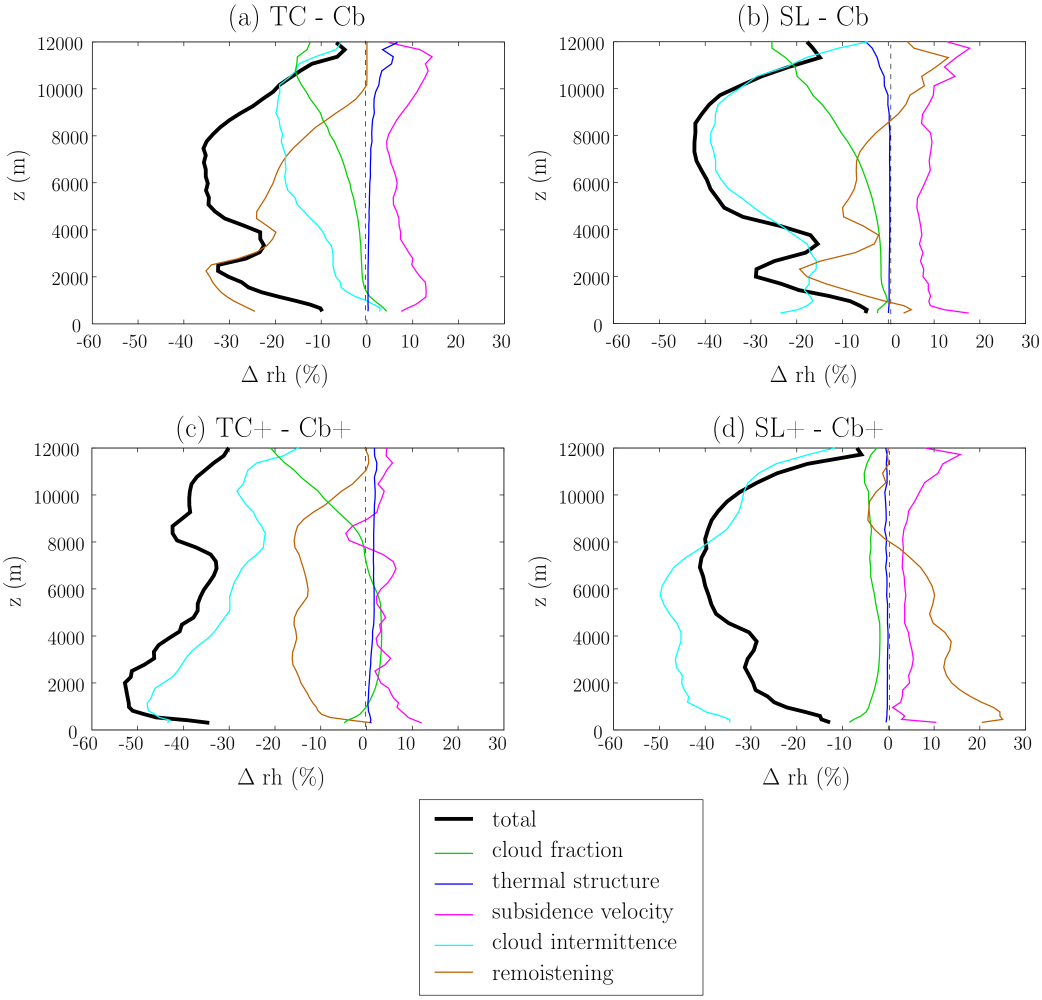

Figure 9. Same as fig 7 but for (a) TC minus Cb, (b) TC+ minus Cb+, (c) SL minus Cb and (d) SL+ minus Cb+. .

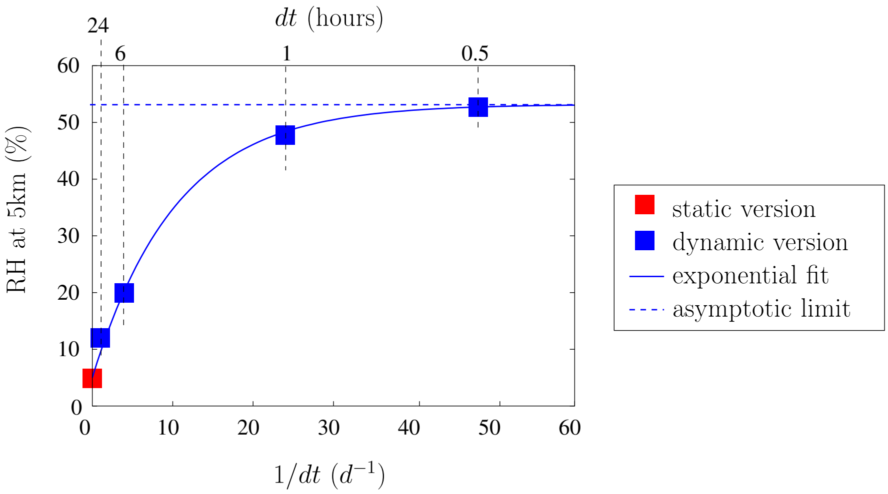

Figure 10. Domain-mean RH predicted by the last-saturation model as a function of the time step dt of the cloud field, for the Cb simulation. The blue markers show values predicted by the last-saturation model without remoistening and the red marker shows the value predicted in the static case. The blue line shows an approximate exponential fit, with initial value corresponding to the static value, asymptotic value of 53.2% and time scale of 2.3 hours.

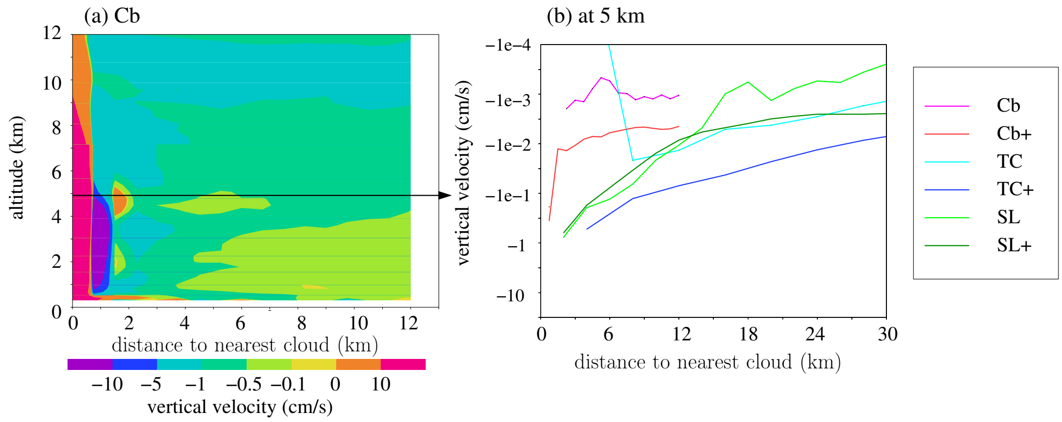

Figure 11. (a) Composite of vertical velocity w, as a function of altitude and of the distance to the nearest cloud for, the Cb simulation. (b) vertical velocity at 5 km as a function of the distance to the nearest cloud, for the 6 simulations.

erally detrained from clouds. We expect that this effect is at least partially accounted for by our calculation of $\left(\frac{\partial q}{\partial t}\right)_{remoist,env}$ as a residual term from the moisture budget.

To summarize, several approximations of the last-saturation model may lead to some biases. However, the capacity of the simple model to capture the RH simulated by the CRM shows that these biases are small, or that they compensate each other. We consider that they are sufficiently small to use the last-saturation model to decompose the RH differences between simulation pairs (section 3.3).

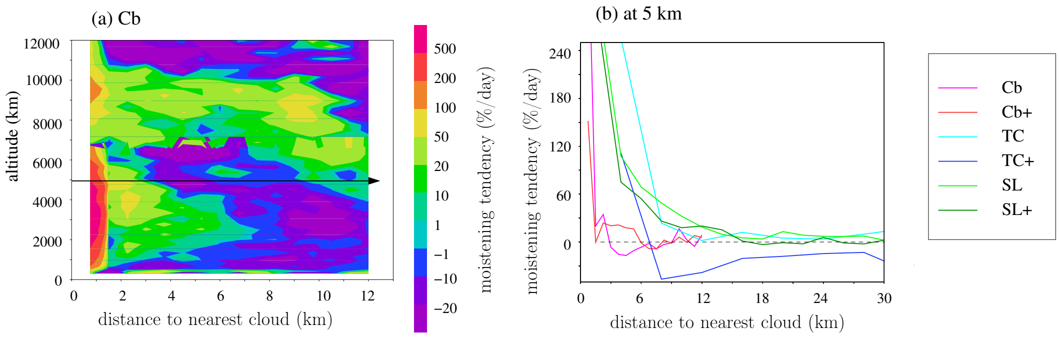

Figure 12. Same as fig 12 but for the the moistening tendency undergone by air parcels subsiding in the environment around clouds. Positive values indicate moistening.

4 Analytical models to understand the cloud intermittence and remoistening contributions

The previous section has shown that the main contribution to the drier troposphere when convection is more aggregated is cloud intermittence. Moistening around clouds by microphysical processes is a secondary contribution. The goal of this section is to design even simpler models for the last-saturation altitude (section 4.1) and for the remoistening term (section 4.2) to help interpret these two contributions.

4.1 Cloud intermittence: key role of the life duration of convective systems

As an indication for the domain-mean RH, we develop an analytical model to estimate the domain-mean last-saturation altitude $\overline{z_{last}}$, where z_{last} is the last altitude where a cloud is encountered as a parcel subsides down to z_0.

4.1.1 Last-saturation altitude as a Markov chain

We denote t_{last} the time of the air parcel descent from z_{last} to z_0, and n_{last} the number of time steps of this descent: $t_{last} = n_{last} \cdot dt$. The number of time steps of the back-trajectory increase as we go back in time.

The probability for n_{last} to be 0 (i.e. $z_{last} = z_0$) is the probability that an air parcel is cloudy at step 0 of the trajectory:

$$P(n_{last} = 0) = P(C_0) \tag{3}$$

where $P(C_n)$ is the probability to be cloudy at trajectory step n. This corresponds to the cloud fraction at the altitude where the trajectory is at trajectory step n.

The probability for n_{last} to be 1 is the probability that an air parcel is cloudy at the 1st trajectory step, and then unsaturated at trajectory step 0:

$$P(n_{last} = 1) = P(C_1 \cap U_0) = P(C_1) \cdot P(U_0|C_1) \tag{4}$$

where $P(U_{n-1}|C_n)$ is the probability that an air parcel is unsaturated at trajectory step $n-1$ knowing that it was cloudy at trajectory step n.

For $n_{last} > 1$, the probability for n_{last} is the probability that an air parcel is cloudy at time step n_{last}, then unsaturated at all trajectory steps from $n_{last} - 1$ to 0:

$$P(n_{last}) = P(C_{n_{last}}) \cdot P(U_{n_{last-1}}|C_{n_{last}}) \cdot \prod_{n=1}^{n_{last}-1} P(U_{n-1}|U_n) \tag{5}$$

where $P(U_{n-1}|U_n)$ is the probability that an air parcel is unsaturated at trajectory step $n-1$ knowing that it was unsaturated at trajectory step n.

The probability distribution for n_{last} can thus be formulated in terms of a Markov chain with transitional probabilities $P(U_{n-1}|U_n)$. This is reminiscent of cloud overlap formulation (Hogan & Illingworth, 2000; Bergman & Rasch, 2002), except that here the overlaps are temporal and not just vertical.

Since $P(C_n|U_{n-1}) = 1 - P(U_n|U_{n-1})$, and using the property that $P(A|B) \cdot P(B) = P(A \cap B)$, we can demonstrate that

$$P(U_{n-1}|U_n) = \left(1 - P(U_{n-1}|C_n) \cdot \frac{P(C_n)}{P(U_{n-1})}\right) \cdot \frac{P(U_{n-1})}{P(U_n)}$$

We assume that the probabilities are stationary and spatially homogeneous, so $P(U_{n-1}) = P(U_n) = 1 - f$ and $P(C_n) = f$, where f is the cloud fraction. We thus get:

$$P(U_{n-1}|U_n) = 1 - P(U_{n-1}|C_n) \cdot \frac{f}{1-f}$$

Therefore, $P(U_{n-1}|U_n)$ can be estimated from $P(U_{n-1}|C_n)$. To calculate the probability distribution of n_{last}, all we need to calculate is $P(U_{n-1}|C_n)$. This is the goal of the next section.

4.1.2 Case of N convective systems of same size and life duration that randomly appear in the domain

The transitional probability $P(U_{n-1}|C_n)$ can directly be diagnosed from the CRM simulations. We find that the estimates along trajectories are virtually identical to estimates ignoring the vertical displacement of air parcels (Fig 13a, dashed lines almost invisible below solid lines). The transitional probabilities are thus determined by the temporal evolution of clouds, not their vertical distribution. This justifies our approximation that convective systems are vertical cylinders (fig 14a). For the sake of simplicity, we assume that the cloud fraction f is vertically uniform along a trajectory. We thus assume that the transitional probabilities are vertically uniform and depend only on the appearance and dissipation of cloud systems. In other words, $P(U_{n-1})$ is the probability of having no cloud at time $n-1$, and $P(C_n)$ is the probability of having a cloud at time n, whatever the altitude. We further assume that there always are N convective systems of the same size and the same life duration D that randomly appear anywhere in the domain, except where there was already a previous convective system (fig 14a).

The probability $P(U_{n-1}|C_n)$ is the probability that the cloud, where the parcel is, dissipates between time steps n and $n-1$. We assume that the probability of dissipation of a system is uniform during its lifetime:

$$P(U_{n-1}|C_n) = \frac{dt}{D} \tag{6}$$

Note that we here assume that dt is sufficiently small so that $dt \leq D$. In the limit case where $dt = D$, then clouds never live longer than a time step, so the probability to have no cloud given that there was no cloud at the previous time step is 1.

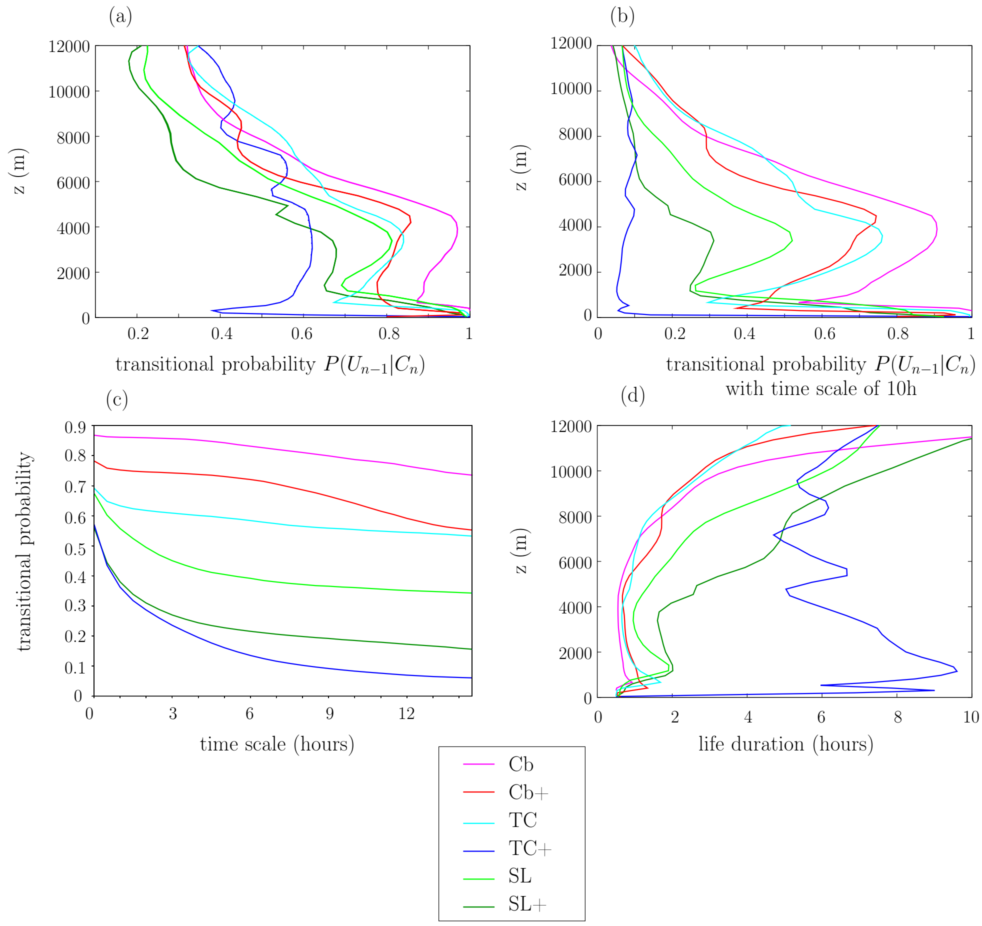

Figure 13. (a) Transitional probability $P(U_{n-1}|C_n)$ along the parcel trajectories (solid) and neglecting the vertical displacement of air parcels (dashed). Dashed lines are almost below solid lines. (b) Transitional probability at the time scale of 10h, i.e. the probability that no clouds appear during the next 10 hours knowing that there was a cloud at a given time step. (c) Transitional probability at 5 km as a function of the time scale over which we check that the cloud does not re-appear. (d) Life duration of clouds based on the transitional probability at the time scale of 10h.

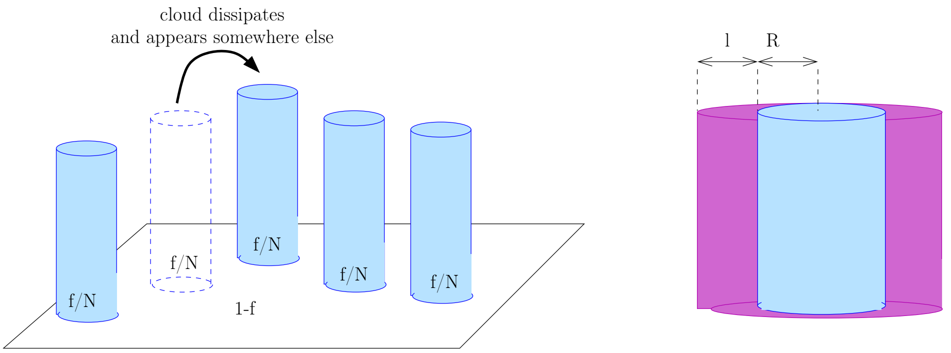

(a) N cylindric clouds (b) cyclindric cloud with its moistening fringe

Figure 14. (a) N convective systems with a cylindrical shape and life duration D dissipate and appear randomly anywhere in the domain except where some convective systems are already present $(1 - f)$. In this schematic, $N = 4$ and $D = 4 \cdot dt$, so that at each time step, one convective system dissipates (dashed blue line) and appears somewhere else. (b) Schematic showing the moistening fringes (purple) around the convective systems.

To summarize, the probability distribution for n_{last} is given by:

$$P(n_{last} = 0) = f \tag{7}$$

For $n_{last} \geq 1$:

$$P(n_{last}) = f \cdot \frac{dt}{D} \cdot \left(1 - \frac{dt}{D} \cdot \frac{f}{1-f}\right)^{n_{last}-1} \tag{8}$$

We can check that:

$$\sum_{n_{last}=0}^{+\infty} P(n_{last}) = f + f \cdot \frac{dt}{D} \cdot \frac{1-0}{1 - 1 + \frac{dt}{D} \cdot \frac{f}{1-f}} = 1$$

4.1.3 Case of uniform subsidence velocity and expression for the last-saturation altitude

If the subsidence velocity of air parcels is vertically uniform, then

$$n_{last} = \frac{z_{last} - z_0}{w_{env} \cdot dt}$$

This allows us to calculate the distribution of z_{last}: for $z_{last} - z_0 < w_{env} \cdot dt$,

$$P(z_{last}) = \frac{f}{dt \cdot w_{env}} \tag{9}$$

and for $z_{last} - z_0 \geq w_{env} \cdot dt$,

$$P(z_{last}) = P(n_{last}) \cdot \frac{dn_{last}}{dz_{last}} = \frac{f}{D \cdot w_{env}} \cdot \left(1 - \frac{dt}{D} \cdot \frac{f}{1-f}\right)^{n_{last}-1} \tag{10}$$

If we assume that $ln\left(1 - \frac{dt}{D} \cdot \frac{f}{1-f}\right) \simeq -\frac{dt}{D} \cdot \frac{f}{1-f}$, we can check again that:

$$\int_{z_{last}=z_0}^{+\infty} P(z_{last}) \cdot dz_{last} = 1$$

This set of equation allows to approximate the distribution of $z_{last} - z_0$ to first order. The shape of the $P(z_{last})$ distribution is reminiscent of that in (Sherwood et al., 2006) where remoistening events followed a random Poisson process.

We now estimate the domain-mean value of z_{last} from this distribution:

$$\overline{z_{last}} = \int_{z_{last}=z_0}^{+\infty} P(z_{last}) \cdot z_{last} \cdot dz_{last}$$

Assuming again that $ln\left(1 - \frac{dt}{D} \cdot \frac{f}{1-f}\right) \simeq -\frac{dt}{D} \cdot \frac{f}{1-f}$ and that $dt \cdot f \ll D \cdot (1-f)$, and performing an integration by parts, we calculate that:

$$\overline{z_{last}} - z_0 \simeq \frac{w_{env} \cdot D \cdot (1-f)^3}{f} \tag{11}$$

We thus expect $\overline{z_{last}}$ to be smaller, and thus the troposphere to be moister, for larger f , for smaller w_{env}, and for larger life duration D. The dominant contribution of the intermittence contribution in section 3.3 suggests that D is a key factor. Its estimate and physical meaning is the subject of the next sub-section.

4.1.4 Estimate and physical meaning of the life duration of convective systems

The transitional probability $P(U_{n-1}|C_n)$ can directly be diagnosed from the CRM simulations (Fig 13a). Since convection in TC+ is strongly aggregated into a single, nearly stationary tropical cyclone, we would expect the transitional probability $P(U_{n-1}|C_n)$ to be very small. However, contrary to expectations, the transitional probability for TC+ is not dramatically smaller than for other simulations (Fig 13a, blue). This is because the transitional probability actually combines two effects: (1) the moving borders of clouds, and (2) the actual dissipation of a convective system. The first effect leads to clouds appearing and disappearing at a very high frequency with little effect on the RH. This effect is however problematic because our simple Markov chain is based on the previous time step only. We would need to account for a longer memory. To more accurately predict the RH, we thus focus on the second effect. We estimate the life duration D based on the probability that no clouds appear during several time steps following a cloud. If we calculate the transitional probability as the probability that no clouds re-appear during the next 10 hours, we can find that consistent with expectations, the smallest transitional probability is by far for TC+, followed by the squall lines (Fig 13b). After 10 hours, the transitional probabilities converge toward some value that correspond to the actual disappearance of convective systems (Fig 13c). We thus use this time scale to estimate the life duration of convective systems, as $D = dt/P(U_{n-1}|C_n)$.

In the mid-troposphere, we obtain life durations of the order of 6 hours for TC+, 3 hours for SL+, 1 hour for SL and 30 minutes for Cb, TC and Cb+ (Fig 13d). For cumulonimbus clouds, this is consistent with what we expect from their life cycles. For TC, the small life duration is also consistent with the relatively disorganized character of this simulation (Fig 2b) For squall lines and TC+, D is smaller than their actual duration (infinite in our simulations), because they propagate. We can show that in case of propagative systems, the same equations hold except that D is replaced by an effective duration $D_{eff} \leq D$ which decreases as systems propagate (SI text S1).

4.1.5 Results and discussion

Using the life duration D as diagnosed from the previous section, we find that the simple scaling from equation 11 is able to qualitatively capture the shape and magnitude of the RH profiles relative to the prediction by the last saturation model without remoistening (fig 15a, compare with fig 5a). In particular, the scaling captures the "C-shape" simulated for the TC, SL and SL+ cases and observed in reality (Romps, 2014). In the scaling, this shape is caused by the maximum cloud fraction in the upper troposphere (fig 8b) and by the minimum cloud life time in the lowest levels (fig 13d). Importantly, the scaling captures the moister RH simulated when the large-scale dynamical regime is more ascending (fig 15c, compare with fig 5c), and the drier RH simulated when convection is more aggregated (fig 15d, compare with fig 5d). The RH profiles predicted by the simple scaling significantly correlate across simulations with those predicted by the last-saturation model without remoistening (fig 15b, solid red). The simple scaling performs almost as well as the RH predicted by the full probability distribution from equation 10 (15b, dashed red).

Using the simple scaling, we can isolate the relative contributions of D, f and w_{env} on the predicted RH, by predicted the RH if only one parameter varies. We find that the contribution of w_{env} opposes the RH differences across simulations (negative correlation for the dashed cyan line in fig 15b). Both D and f combine to explain the RH differences across simulations (positive correlations for the dashed blue and magenta lines in fig 15b). We find that variations in f explain most of the variations in RH when the large-scale ascent varies, while variations in D explain most of the variations in RH when the convective aggregation varies (not shown). This supports the idea that the longer duration of convective systems is the main factor responsible for the drier RH when convection is more aggregated.

We note that $\overline{z_{last}}$ does not depend on N, but on D: it depends on the cloud intermittence, but not at all on the spatial arrangement of clouds. In addition, we find that this result would be unchanged even if some fraction of the domain never experiences convection (SI text S2). These results support hypothesis #2b (cloud intermittence) and contradict hypothesis #2a (spatial arrangement).

4.2 Remoistening by microphysical processes: role of spatial aggregation

We have shown that the remoistening around clouds significantly contributes to the moister troposphere when convection is more disorganized, consistent with hypothesis #1. We now aim at better understanding, at least qualitatively, this contribution.

The contribution of the remoistening around clouds ($h_{dyn,remoist}-h_{dyn}$, not shown) reflects the remoistening tendency in average over the environment around clouds ($\left(\frac{\partial q}{\partial t}\right)_{remoist,env}$, Fig 8a). The composite of the remoistening term as a function of the distance to the nearest cloud shows that the moistening tendency is strongest in the vicinity of clouds and decays away from clouds (Fig 12). It is thus mainly restricted to a "moistening fringe" around clouds (Fig 12), consistent with the hypothesis of (Windmiller & Craig, 2019) of a finite zone around clouds where the air is moistened. Assuming that the remoistening tendency exclusively occurs in the moistening fringes, the remoistening tendency in average over the environment can be written as:

$$\left(\frac{\partial q}{\partial t}\right)_{remoist,env} = \frac{A_{fringe}}{A_{env}} \cdot \left(\frac{\partial q}{\partial t}\right)_{remoist,fringe}$$

where A_{fringe} is the area of the domain covered by the moistening fringe, A_{env} is the area of the domain covered by the environment, and $\left(\frac{\partial q}{\partial t}\right)_{remoist,fringe}$ the moist-

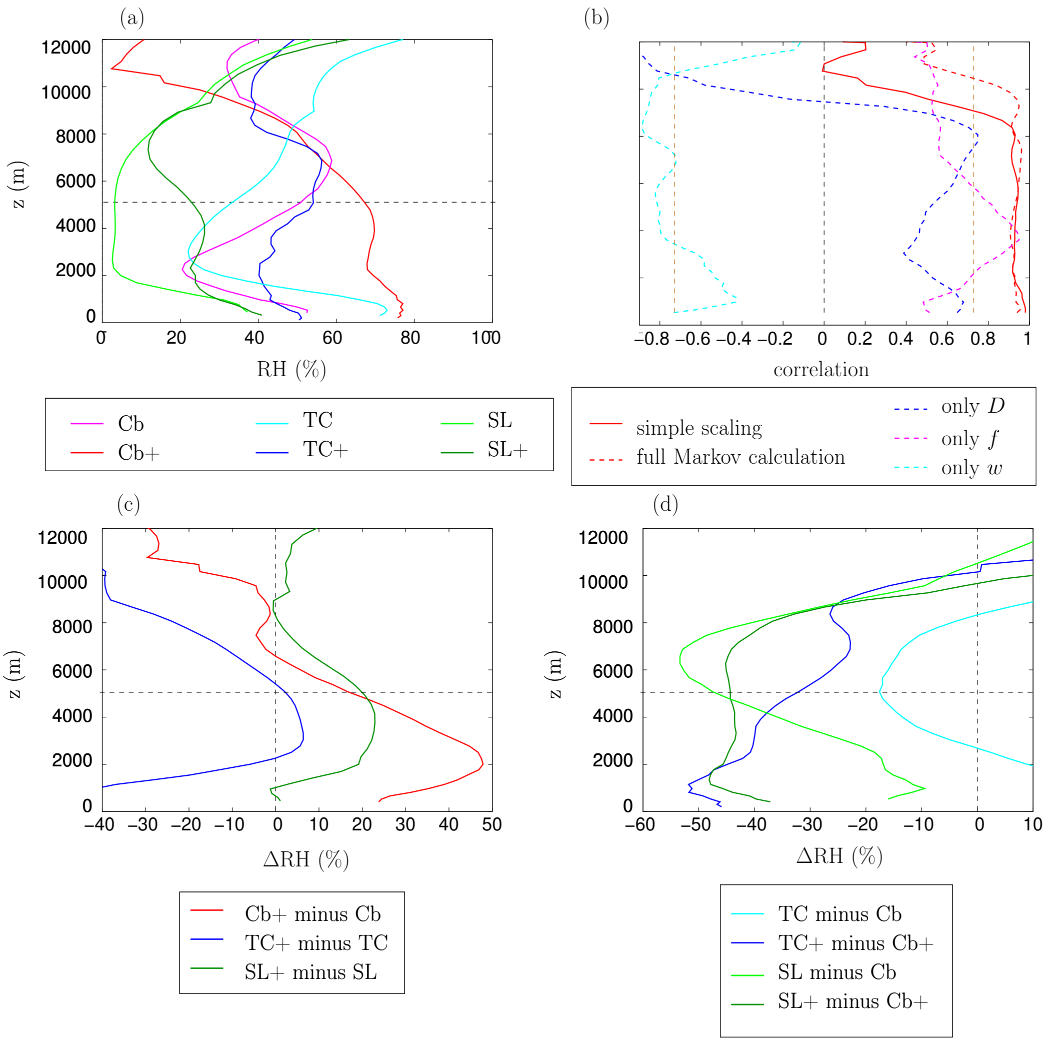

Figure 15. (a) Vertical profiles of domain-mean RH predicted by the simple scaling from equation 11. (b) Correlation coefficient as a function of altitude between the domain-mean RH predicted by the simple scaling from equation 11 (solid red) and that predicted by the last-saturation model without remoistening, across the 6 simulations. The vertical dashed brown line indicates the correlation threshold for statistical significance at 90%. The dashed red line shows the correlation coefficient for the RH predicted by the full probability distribution (equation 10). The dashed blue, magenta and cyan line show the correlation coefficient for the RH predicted by the simple scaling if only D, f and w vary respectively. (c-d) Same as figures 5c-d but for the RH predicted by the simple scaling.

ening tendency in the moistening fringes. Let's note L the length of the domain, $l \ll L$ the thickness of the fringes and $\eta = N/L^2$ the density of clouds. For the sake of simplicity, we assume that all clouds are identical with a radius R, such that the cloud fraction f is:

$$f = \eta \pi R^2$$

We thus have:

$$A_{env} = L^2 \cdot (1 - f)$$

and

$$A_{fringe} = N \cdot \left(\pi(R + l)^2 - \pi R2\right) \simeq 2N\pi Rl = 2 \cdot f \cdot L^2 \cdot l \cdot \sqrt{\eta \cdot \pi}$$

Thus

$$\left(\frac{\partial q}{\partial t}\right)_{remoist,env} = \frac{2 \cdot f \cdot l \cdot \sqrt{\eta \cdot \pi}}{(1 - f)} \cdot \left(\frac{\partial q}{\partial t}\right)_{remoist,fringe}$$

We thus expect the $\left(\frac{\partial q}{\partial t}\right)_{remoist,env}$ to scale with $\sqrt{\eta}$, i.e. with the density of clouds in the domain. This is why the remoistening term systematically contributes to a moister troposphere when convection is more disaggregated. In contrast to the intermittence contribution which is tied to the duration of convective systems, the remoistening contribution is directly tied to the spatial aggregation as is more frequently studied (e.g. (Tobin et al., 2012)).

We also expect the remoistening term to scale with f, and thus to contribute to the moister troposphere when the large-scale dynamical regime is more ascending. However, the other factors, i.e. l and $\left(\frac{\partial q}{\partial t}\right)_{remoist,fringe}$, are related to the meso-scale dynamics of the convective systems and probably also to the spatial resolution. Predicting them is beyond the scope of this paper, and this probably explains why the moistening contribution strongly varies depending on the dynamical regime and organization type.

5 Summary and discussion

To summarize, the drier environment when convection is more aggregated that has been observed in self-aggregation simulations (Bretherton et al., 2005) remains true in simulations with forced types of convective organization (cyclones, squall lines). A simple last-saturation model captures the drier environment in more aggregated simulations. Using this simple model, we show that the main mechanisms explaining why the troposphere is drier in the case of tropical cyclones and squall lines in our CRM simulations is the cloud intermittence. According to the last-saturation paradigm, when clouds are more intermittent, the probability for air parcels to meet clouds as they descend is larger (fig 1, blue). We built an analytical model that highlights the key importance of D, the time scale during which convective systems remain at the same location. It corresponds to the duration of convective systems, and can be reduced if they propagate.

The last-saturation paradigm has proven successful in simulating the RH response to the large-scale circulation (Sherwood, 1996; Pierrhumbert & Roca, 1998; Dessler & Sherwood, 2000). We show here that it is also successful in simulating the RH response to convective organization.

Moistening of the environment by microphysical processes is more effective when the number of clouds is larger, due to a larger interface area between clouds and the environment (fig 1, purple). This was hypothesized by (Tobin et al., 2012) and contributes positively to the drying in aggregated simulations, but this effect is secondary. This effect scales with the square root of the density of convective systems in the domain, i.e. is determined by spatial aggregation.

Apart from the secondary effect of microphysical processes, we show that the spatial aggregation in itself has little impact on the domain-mean RH. The key mechanism is cloud intermittence, i.e. the temporal distribution of clouds. If the tropical cyclone had a life duration as short as isolated Cb clouds, the troposphere around it would be as moist as in the disaggregated case. Conversely, if the isolated Cb were stationary, the troposphere around it would be as dry as in the cyclone case. In reality, the size and life duration of convective system are related (Roca et al., 2017). This probably explains why spatially aggregated convection is associated with a drier environment: aggregated convection is statistically associated with longer-lived convective system. Therefore, we hypothesize that the observed correlation between spatial aggregation and tropospheric dryness is actually mainly mediated by the life duration of convective systems. Future studies are necessary to observationally confirm this hypothesis. Our analytical model also suggests that propagative systems such as squall lines or cyclones would be associated with higher RH than non-propagative systems of similar size and duration. This also remains to be observationally assessed.

Finally, the idealized setting of the simulation prevented us from assessing the impact of large-scale horizontal advection on the tropospheric humidity. The relative importance of large-scale advection and local convective processes in explaining the observed correlation between spatial aggregation and tropospheric dryness will have to be quantified in global CRM simulations, such as those performed as part of the DYAMOND project (Stevens et al., 2019). In a future study, the last-saturation framework proposed here could be adapted to account for large-scale advection in such global simulations.

Acknowledgments

This work was granted access to the HPC resources of TGCC under the allocation 2092 made by GENCI. C.M. gratefully acknowledges funding from the European Research Council (ERC) under the European Union's Horizon 2020 research and innovation program (Project CLUSTER, grant agreement No 805041). C.R. and C.M. acknowledge funding from the INSU/LEFE project LEFE2021 SAMiso. F.L. contributed as part of his internship as a Master student at Universit Paris Saclay and was funded by the project CLUSTER. E. N.-B. contributed as part of his internship as a student at Sorbonne Universit. We are grateful for discussions with Raphael Lebrun, Jean-Louis Dufresne and Sandrine Bony. Information on SAM can be found on this web page:

http://rossby.msrc.sunysb.edu/~marat/SAM.html. All simulation outputs used in this article will be submitted to the PANGEA data repository.

References

Abramian, S., Muller, C., & Risi, C. (2022). Shear-convection interactions and orientation of tropical squall lines. *Geophysical Research Letters*, *49*(1), e2021GL095184.

Bergman, J. W., & Rasch, P. J. (2002). Parameterizing vertically coherent cloud distributions. *Journal of the atmospheric sciences*, *59*(14), 2165–2182.

Beucler, T., Leutwyler, D., & Windmiller, J. M. (2020). Quantifying convective aggregation using the tropical moist margin's length. *Journal of Advances in Modeling Earth Systems*, *12*(10), e2020MS002092.

Bony, S., Stevens, B., Coppin, D., Becker, T., Reed, K., Voigt, A., & Medeiros, B.

(2016). Thermodynamic control of anvil-cloud amount. *Proc. Natl. Acad. Sci.*, *113 (32)*, 8927?8932, 10.1073/pnas.1601472113.

Bretherton, C. S., Blossey, P. N., & Khairoutdinov, M. (2005). An Energy-Balance Analysis of Deep Convective Self-Aggregation above Uniform SST. *J. Atmos. Sci.*, *62*, 4273-4292.

Bretherton, C. S., Peters, M. E., & Back, L. E. (2004). Relationships between water vapor path and precipitation over the tropical oceans. *Journal of climate*, *17*(7), 1517–1528.

Bretherton, C. S., & Smolarkiewicz, P. K. (1989). Gravity waves, compensating subsidence and detrainment around cumulus clouds. *Journal of Atmospheric Sciences*, *46*(6), 740–759.

Chavas, D. R., & Emanuel, K. (2014). Equilibrium tropical cyclone size in an idealized state of axisymmetric radiative–convective equilibrium. *Journal of the Atmospheric Sciences*, *71*(5), 1663–1680.

Craig, G. C. (1996). Dimensional analysis of a convecting atmosphere in equilibrium with external forcing. *Quarterly Journal of the Royal Meteorological Society*, *122*(536), 1963–1967.

Dessler, A. E., & Sherwood, S. C. (2000). Simulations of tropical upper tropospheric humidity. *J. Geophys. Res.*, *105 (D15)*, 20,155-20,263.

Diongue, A., Lafore, J.-P., Redelsperger, J.-L., & Roca, R. (2002). Numerical study of a sahelian synoptic weather system: Initiation and mature stages of convection and its interactions with the large-scale dynamics. *Quarterly Journal of the Royal Meteorological Society: A journal of the atmospheric sciences, applied meteorology and physical oceanography*, *128*(584), 1899–1927.

Emanuel, K. (2019). Inferences from simple models of slow, convectively coupled processes. *Journal of the Atmospheric Sciences*, *76*(1), 195–208.

Gamache, J. F., & Houze, R. A. (1981). Mesoscale air motions associated with a tropical squall line. *monthly weather review*, *110*, 118-135.

Gentry, M. S., & Lackmann, G. M. (2010). Sensitivity of simulated tropical cyclone structure and intensity to horizontal resolution. *Monthly Weather Review*, *138*(3), 688–704.

Glenn, I. B., & Krueger, S. K. (2014). Downdrafts in the near cloud environment of deep convective updrafts. *Journal of Advances in Modeling Earth Systems*, *6*(1), 1–8.

Held, I. M. (2005). The gap between simulation and understanding in climate modeling. *Bulletin of the American Meteorological Society*, *86*(11), 1609–1614.

Hogan, R. J., & Illingworth, A. J. (2000). Deriving cloud overlap statistics from radar. *Quarterly Journal of the Royal Meteorological Society*, *126*(569), 2903–2909.

Houze, R. A. (2004). Mesoscale convective systems. *Rev. Geophys.*, *42 (4)*, DOI: 10.1029/2004RG000150.

Houze, R. A. (2010). Clouds in tropical cyclones. *Monthly Weather Review*, *138*(2), 293–344.

Houze Jr, R. A., & Betts, A. K. (1981). Convection in gate. *Reviews of Geophysics*, *19*(4), 541–576.

Jakob, C., Singh, M., & Jungandreas, L. (2019). Radiative convective equilibrium and organized convection: An observational perspective. *Journal of Geophysical Research: Atmospheres*, *124*(10), 5418–5430.

Johnson, R. H., Rickenbach, T. M., Rutledge, S. A., Ciesielski, P. E., & Schubert, W. H. (1999). Trimodal characteristics of tropical convection. *Journal of climate*, *12*(8), 2397–2418.

Khairoutdinov, M., & Emanuel, K. (2013). Rotating radiative-convective equilibrium simulated by a cloud-resolving model. *Journal of Advances in Modeling Earth Systems*, *5*(4), 816–825.

Khairoutdinov, M., & Randall, D. A. (2003). Cloud resolving modeling of the ARM summer 1997 IOP: Model formulation, results, uncertainties, and sensitivities. *Journal of the Atmospheric Sciences*, *60*(4), 607–625.

Mapes, B., & Neale, R. (2011). Parameterizing convective organization to escape the entrainment dilemma. *Journal of Advances in Modeling Earth Systems*, *3*(2).

Mauritsen, T., & Stevens, B. (2015). Missing iris effect as a possible cause of muted hydrological change and high climate sensitivity in models. *Nature Geoscience*, *8*(5), 346–351.

Moncrieff, M. W. (2019). Toward a dynamical foundation for organized convection parameterization in gcms. *Geophysical Research Letters*, *46*(23), 14103–14108.

Muller, C. (2013). Impact of convective organization on the response of tropical precipitation extremes to warming. *Journal of climate*, *26*(14), 5028–5043.

Muller, C., & Held, I. M. (2012). Detailed investigation of the self-aggregation of convection in cloud-resolving simulations. *J. Atmos. Sci.*, *69*, 2551-2565, doi: http://dx.doi.org/10.1175/JAS-D-11-0257.1.

Muller, C., & Romps, D. M. (2018). Acceleration of tropical cyclogenesis by self-aggregation feedbacks. *Proceedings of the National Academy of Sciences*, 201719967.

Muller, C., Yang, D., Craig, G., Cronin, T., Fildier, B., Haerter, J. O., ... others (2022). Spontaneous aggregation of convective storms. *Annual Review of Fluid Mechanics*, *54*, 133–157.

Pierrhumbert, R. T., & Roca, R. (1998). Evidence for control of atlantic subtropical humidity by large scale advection. *Geophys. Res. Lett.*, *25*, 4537-4540.

Risi, C., Muller, C., & Blossey, P. (2021). Rain evaporation, snow melt, and entrainment at the heart of water vapor isotopic variations in the tropical troposphere, according to large-eddy simulations and a two-column model. *Journal of advances in modeling earth systems*, *13*(4), e2020MS002381.

Risi, C., Muller, C., & N, B. P. (2020). What controls the water vapor isotopic composition near the surface of tropical oceans? Results from an analytical model constrained by large-eddy simulations. *Journal of Advances in Modeling Earth Systems*.

Robe, F. R., & Emanuel, K. A. (2001). The effect of vertical wind shear on radiative–convective equilibrium states. *Journal of the atmospheric sciences*, *58*(11), 1427–1445.

Roca, R., Aublanc, J., Chambon, P., Fiolleau, T., & Viltard, N. (2014). Robust observational quantification of the contribution of mesoscale convective systems to rainfall in the tropics. *Journal of Climate*, *27*(13), 4952–4958.

Roca, R., Fiolleau, T., & Bouniol, D. (2017). A simple model of the life cycle of mesoscale convective systems cloud shield in the tropics. *Journal of Climate*, *30*(11), 4283–4298.

Roca, R., Lafore, J.-P., Piriou, C., & Redelsperger, J.-L. (2005). Extratropical dry-air intrusions into the West African monsoon midtroposphere: an important factor for the convective activity over the Sahel. *J. Atmos. Sci.*, *62*, 390-407.

Romps, D. M. (2014). An analytical model for tropical relative humidity. *Journal of Climate*, *27*(19), 7432–7449.

Romps, D. M. (2021). Ascending columns, wtg, and convective aggregation. *J. atm. sci.*, *78*, 497-508.

Ryoo, J.-M., Igusa, T., & Waugh, D. W. (2009). Pdfs of tropical tropospheric humidity: Measurements and theory. *Journal of climate*, *22*(12), 3357–3373.

Sherwood, S. (1996). Maintenance of the free tropospheric tropical water vapor distribution. part II: simulation of large-scale advection. *J. Clim.*, *11*, 2919-2934.

Sherwood, S., Kursinki, E. R., & Read, W. G. (2006). A distribution law for free-tropospheric relative humidity. *J. Clim.*, *19*, 6267-6277.

Sherwood, S., Roca, R., Weckwerth, T. M., & Andronova, N. G. (2010). Tropospheric water vapor, convection, and climate. *Rev. Geophys.*, *48*.

Singh, M. S., Warren, R. A., & Jakob, C. (2019). A steady-state model for the relationship between humidity, instability, and precipitation in the tropics. *Journal of Advances in Modeling Earth Systems*, *11*(12), 3973–3994.

Stein, T. H., Holloway, C. E., Tobin, I., & Bony, S. (2017). Observed relationships between cloud vertical structure and convective aggregation over tropical ocean. *Journal of Climate*, *30*(6), 2187–2207.

Stevens, B. (2006). Bulk boundary-layer concepts for simplified models of tropical dynamics. *Theoretical and Computational Fluid Dynamics*, *20*(5-6), 279–304.

Stevens, B., Satoh, M., Auger, L., Biercamp, J., Bretherton, C. S., Chen, X., ... others (2019). Dyamond: The dynamics of the atmospheric general circulation modeled on non-hydrostatic domains. *Progress in Earth and Planetary Science*, *6*(1), 61.

Tan, J., Jakob, C., & Lane, T. P. (2013). On the identification of the large-scale properties of tropical convection using cloud regimes. *Journal of Climate*, *26*(17), 6618–6632.

Thompson, G., Field, P. R., Rasmussen, R. M., & Hall, W. D. (2008). Explicit forecasts of winter precipitation using an improved bulk microphysics scheme. part ii: Implementation of a new snow parameterization. *Monthly Weather Review*, *136*(12), 5095–5115.

Tobin, I., Bony, S., Holloway, C. E., Grandpeix, J.-Y., Seze, G., Coppin, D., ... Roca, R. (2013). Does convective aggregation need to be represented in cumulus parameterizations? *Journal of Advances in Modeling Earth Systems*, *5*(4), 692–703.

Tobin, I., Bony, S., & Roca, R. (2012). Observational evidence for relationships between the degree of aggregation of deep convection, water vapor, surface fluxes and radiation. *Journal of Climate*.

Warren, R. A., Singh, M. S., & Jakob, C. (2020). Simulations of radiative-convective-dynamical equilibrium. *Journal of Advances in Modeling Earth Systems*, *12*(3), e2019MS001734.

Windmiller, J. M., & Craig, G. C. (2019). Universality in the spatial evolution of self-aggregation of tropical convection. *Journal of Atmospheric Sciences*, *76*(6), 1677–1696.

Wing, A., Camargo, S. J., & Sobel, A. H. (2016). Role of radiative–convective feedbacks in spontaneous tropical cyclogenesis in idealized numerical simulations. *Journal of the Atmospheric Sciences*, *73*(7), 2633–2642.

Wing, A., Emanuel, K., Holloway, C., & Muller, C. (2017). Convective self-aggregation in numerical models. *Surv. Geophysics.*, *38*, 1173. https://doi.org/10.1007/s10712-017-9408-4.

Supporting Information for "What mechanisms explain the tropospheric drying associated with convective organization? Insights from cloud-resolving and last-saturation models"

Camille Risi [1], Felix Langot [1], Esteban Nocet-Binois[1], Caroline Muller [1,2]

[1]Laboratoire de Meteorologie Dynamique, IPSL, CNRS, Ecole Normale Superieure, Sorbonne Universite, PSL Research University, Paris, France

[2]Institute of Science and Technology Austria, Klosterneuburg, Austria

Contents of this file

1. Text S1: Supplementary calculations for the analytical model: Case of propagative systems
2. Text S2: Supplementary calculations for the analytical model: Case of convective systems restricted on a fraction of the domain
3. Videos V1: Videos of precipitable water maps during the 6 simulations
4. Video V2: Video illustrating the importance of cloud intermittence on the relative humidity

Introduction

This supporting information contains some supplementary calculations for the analytical model, and some videos.

Text S1: Supplementary calculations for the analytical model: Case of propagative systems

To make the calculation easier, here we assume that convective systems have a square shape. We assume that there are N square convective systems of length l with a life duration D and propagating at a speed v (fig S1a).

$$N \cdot l^2 = f \cdot L^2$$

So $l = L \cdot \sqrt{f/N}$.

The area of each cloud that moves away at each time step is:

$$a = v \cdot dt \cdot l = v \cdot dt \cdot L \cdot \sqrt{f/N}$$

The probability of being unsaturated knowing that it was cloudy at the previous time step is the probability that the cloud disappears or moves away.

$$P(U_{n-1}|C_n) = \frac{dt}{D} + (1 - \frac{dt}{D}) \cdot \frac{v \cdot dt \cdot L \cdot \sqrt{f/N}}{l^2} = \frac{dt}{D} + (1 - \frac{dt}{D}) \cdot \frac{v \cdot dt \cdot}{L \cdot \sqrt{f/N}}$$

Let's define D_p the characteristic time scale of the propagation:

$$D_p = \frac{L \cdot \sqrt{f/N}}{v}$$

D_p reflects the time it takes for convective systems to cross the domain. It tends towards $+\infty$ if convective systems do not propagate.

Therefore,

$$P(U_{n-1}|C_n) = \frac{dt}{D} + (1 - \frac{dt}{D}) \cdot \frac{dt}{D_p} = \frac{dt}{D_{eff}}$$

where

$$D_{eff} = D \cdot \frac{1}{1 + (D - dt)/D_p}$$

D_{eff} represents an effective life duration, which is reduced compared to D in case of propagation.

We thus find exactly the same expressions for $P(U_{n-1}|C_n)$ as given in equation **??**, except that D is replaced by D_{eff}.

Text S2: Supplementary calculations for the analytical model: Case of convective systems restricted on a fraction of the domain

In previous studies, the fraction of the domain that was far from any cloud and that never experiences convection was considered a determinant factor in controlling the domain-mean RH (Romps, 2021). To check whether this is the case in our analytical model, we consider the case of N convective systems as in section **??**, but we assume that they can never appear in a fraction g of the domain that is forbidden to them (fig S1b). The probability $P(U_{n-1}|C_n)$ is unchanged since it does not matter where clouds are located in the domain.

Videos V1: Videos of precipitable water maps during the 6 simulations

1. Cb: PWmap_Cb_grads.avi
2. Cb+: PWmap_Cb_m60hPad_grads.avi
3. TC: PWmap_cyclone_grads.avi
4. TC+: PWmap_cyclone_m60hPad_grads.avi
5. SL: PWmap_LdG_grads.avi
6. SL+: PWmap_LdG_m60hPad_grads.avi

Video V2: Video illustrating the importance of cloud intermittence on the relative humidity

rh_video_son.mp4

References

Romps, D. M. (2021). Ascending columns, wtg, and convective aggregation. *J. atm. sci.*, *78*, 497-508.

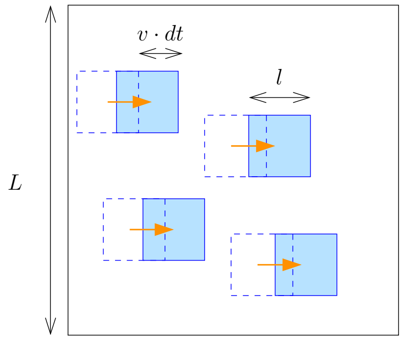

(a) N square propagating clouds

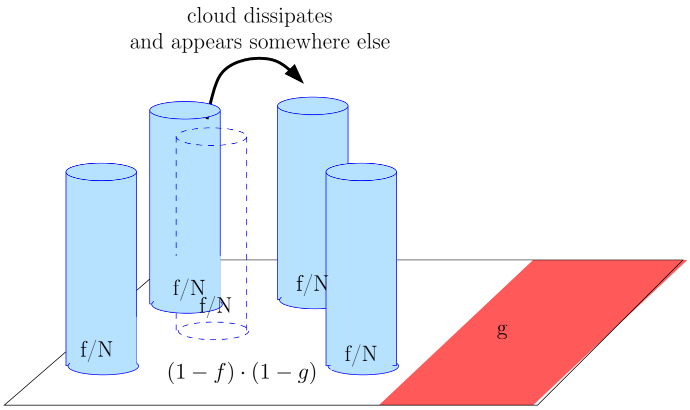

(b) N cylindric clouds with forbidden area

Figure S1. (a) N convective systems with a square shape and life duration D propagate across a domain with propagation speed v. (b) N convective systems with a cylindrical shape and life duration D dissipate and appear randomly across the domain, except in a fraction g of the domain that is forbidden to them (red)